

# Tracing Human Stress from Physiological Signals using UWB Radar

Jia Xu, *Member, IEEE*, Teng Xiao, Pin Lv\*, *Member, IEEE*, Zhe Chen, *Member, IEEE*, Chao Cai, *Member, IEEE*, Yang Zhang, Zehui Xiong

**Abstract**—Stress tracing is an important research domain that supports many applications, such as health care and stress management; and its closest related works are derived from stress detection. However, these existing works cannot well address two important challenges facing stress detection. First, most of these studies involve asking users to wear physiological sensors to detect their stress states, which has a negative impact on the user experience. Second, these studies have failed to effectively utilize multimodal physiological signals, which results in less satisfactory detection results. This paper formally defines the stress tracing problem, which emphasizes the continuous detection of human stress states. A novel deep stress tracing method, named DST, is presented. Note that DST proposes tracing human stress based on physiological signals collected by a noncontact ultra-wideband radar, which is more friendly to users when collecting their physiological signals. In DST, a signal extraction module is carefully designed at first to robustly extract multimodal physiological signals from the raw RF data of the radar, even in the presence of body movement. Afterward, a multimodal fusion module is proposed in DST to ensure that the extracted multimodal physiological signals can be effectively fused and utilized. Extensive experiments are conducted on three real-world datasets, including one self-collected dataset and two publicity datasets. Experimental results show that the proposed DST method significantly outperforms all the baselines in terms of tracing human stress states. On average, DST averagely provides a 6.31% increase in detection accuracy on all datasets, compared with the best baselines.

**Index Terms**—stress tracing, contactless sensing, UWB radar, multimodal fusion, information exchange.

## I. INTRODUCTION

**S**Tress is a feeling of physical or mental tension or anxiety that people encounter in the case of unavoidable conditions or any thought that makes them restless, angry, and frustrated [1], [2]. There is evidence that stress is one of the major factors of various physiological and psychological diseases [3], [4]. Therefore, it is extremely critical to design effective methods to trace the evolution of the human stress state to help individuals manage their stress and help health

care professionals refine their treatments for stress-related diseases.

The closest line of work to the stress tracing problem is the stress detection problem, which is an emerging and important research area for developing advanced computational systems to detect, model, and recognize mental stress states. Since mental stress is frequently accompanied by physical and physiological changes, a person's stress can generally be detected by monitoring and fusing his or her relevant human signals which can be captured by sensor devices [5], [6]. In recent years, many works on stress detection have been proposed by researchers and can be divided into two main categories, namely, traditional machine learning-based methods [7]–[10] and deep learning-based methods [11]–[15]. Compared with the traditional machine learning based methods, works proposed based on deep neural networks have the advantages of higher performance, effective scaling of data, no feature engineering, and strong adaptability [16]–[22], which makes them the mainstream paradigm for stress detection. In addition to applying deep learning, researchers have also attempted to utilize more types of human signals to further improve the quality of stress detection [23], [24]. These signals either reflect human physical states (i.e., physical signals) or are related to human physiological states (i.e., physiological signals). Detecting mental stress via physical signals (such as body postures and facial expressions), however, is deemed to be less reliable since it is relatively easy for a human to control physical signals to hide his or her true stress, especially during social interactions [25]. Under such circumstances, many works prefer to use physiological signals (such as an electrocardiogram (ECG), heart rate (HR), and respiratory rate (RR)) to achieve stress detection since physiological signals can detect stress in a modest, inexpensive, convenient, and easy-to-utilize manner. Although existing stress detection methods based on physiological signals have achieved promising results, they have two crucial limitations:

- 1) *Being unfriendly to users.* To collect physiological signals, users are mostly required to wear physiological sensors (such as ECG detectors, blood pressure monitors, oximeters, and Empatica E4 wrist bands [26]). However, the vast majority of users are reluctant to wear such devices because of the potential risks of privacy disclosure and skin irritation or because of interference with their movements [27].
- 2) *These methods fail to utilize effectively multimodal physiological signals.* It is widely known that different

Jia Xu, Pin Lv are with Guangzhou University, Guangzhou, China (e-mail: xujia@gzhu.edu.cn, lvpin@gzhu.edu.cn), and Teng Xiao is with Guangxi University, Nanning, China (e-mail: xiaoteng@st.gxu.edu.cn). Zhe Chen is with the Intelligent Networking and Computing Research Center, and the School of Computer Science, Fudan University, Shanghai, China (e-mail: zhechen@fudan.edu.cn). Chao Cai is with Huazhong University of Science and Technology, Wuhan, China (e-mail: chriscai@hust.edu.cn). Yang Zhang is with Nanjing University of Aeronautics and Astronautics, Nanjing, China (e-mail: yangzhang@nuaa.edu.cn). Zehui Xiong is with Singapore University of Technology and Design, Singapore (e-mail: zehui\_xiong@sutd.edu.sg). Corresponding author is Pin Lv.

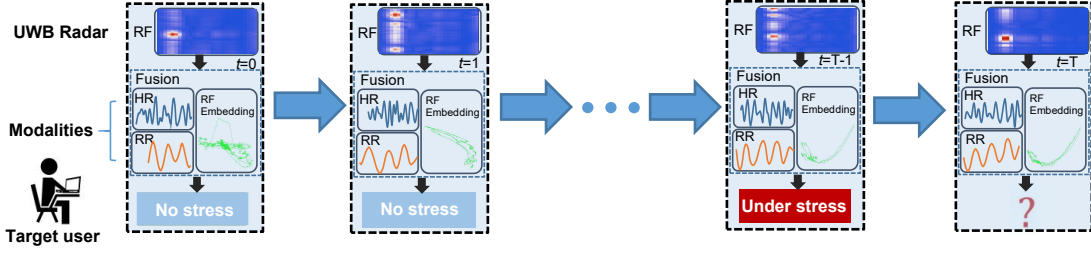


Fig. 1. An illustration of the stress tracing procedure based on multimodal physiological signals using UWB radar

modalities of physiological signals (e.g., HR and RR) contain different information and thus can be jointly utilized to improve stress detection performance [28]. However, current studies mostly directly utilize multimodal physiological signals, i.e., simply selecting the most robust modality of physiological signals [10] or simply fusing multimodal physiological signals via a Multilayer Perceptron Neural network (MLP) (or Convolutional Neural Networks (CNN) [29]) [13], which restricts the improvement in their stress detection performance.

Although a few works [30], [31] that provide solutions for stress detection based on wireless signals and successfully improve user experience have recently been proposed, these works consistently fail to utilize effectively multimodal signals to optimize the detection of human stress and thus can only generate less satisfactory detection results. In this paper, we propose a novel deep learning-based method for tracing human stress based on physiological signals called **Deep Stress Tracing (DST)**. In contrast to most related works, DST is designed to detect the stress states of a target user in a continuous manner. As shown in Figure 1, DST takes a target user's multimodal physiological signals (i.e., HR and RR), which are derived by decomposing the RF data collected via an ultra-wideband (UWB) radar, which is a contactless sensor widely used in wireless sensing [32]–[34] as the inputs and can continuously trace the change in the user's stress state (i.e., no stress or under stress). Using UWB radar is the key to addressing the first limitation since UWB radar can collect a target user's HR and RR signals in a noncontact manner. Moreover, UWB radar has many advantages in handling stress detection tasks. For example, it has low energy consumption and higher compliance, is not affected by lighting or other physical obstacles, is less susceptible to noise, has fewer privacy issues, and does not have complex equipment deployment [35].

To address the second limitation, DST designs a deep neural architecture that optimizes the extraction and utilization of multimodal physiological signals for effective stress tracing. Specifically, following the idea in [36], a **Signal Extraction Module (SEM)** is designed to optimize the extraction of HR and RR signals from RF data. The SEM is very robust. On one hand, the SEM can still extract high-quality HR and RR signals when the HR and RR signals interfere with each other. On the other hand, unintentional body movements, which have a negative impact on the parameter estimation

of physiological movements (i.e., heartbeat and breathing), are adequately handled by the SEM. Then, to better fuse and utilize the multimodal physiological signals (i.e., HR and RR) extracted by the SEM, a **Multimodal Fusion Module (MFM)** is presented in DST. Specifically, the MFM utilizes a modular and flexible approach to effectively fuse three types of feature streams, i.e., HR signals, RR signals, and original RF data, which contain rich information such as head movements and body postures of the target user. Moreover, to ensure that the physiological changes detected at the time of measurement are caused by stress, in this study, we defined a stress induction protocol and used the Depression Anxiety Stress Scale (DASS) [37] to verify the effectiveness of the protocol. The main contributions of this paper are summarized as follows:

- We formally define the problem of stress tracing, which is very important for supporting many practical applications, such as health and stress management.
- We propose a novel stress tracing method, called Deep Stress Tracing (DST), which effectively traces human stress from physiological signals gathered by a contactless UWB radar. Compared with most related methods, DST is more friendly to users since users are not required to wear any physiological sensors during the stress monitoring procedure. Moreover, DST better exploits multimodal physiological signals and thus improves the detection accuracy compared with related methods built based on contactless radars.
- We design several modules in DST, namely, the Signal Extraction Module (SEM) and Multimodal Fusion Module (MFM), to ensure that the multimodal physiological signals of a target user are effectively extracted, fused, and utilized to optimize the stress tracing tasks.
- The effectiveness of the proposed DST method for stress tracing is carefully evaluated using three real-world datasets. The experimental results verify the superiority of DST compared with all baselines and the good generalization of DST in handling different multimodal datasets.

The remainder of the paper is organized as follows : Section II analyzes related works. Section III provides preliminaries, where the stress tracing problem is formally defined. Section IV elaborates the implementation of the proposed Deep Stress Tracing (DST) method. Section V discusses the experimental settings and results. Section VI is dedicated to discussing the research findings and future work.

## II. RELATED WORKS

The closest line of work to the stress tracing problem investigated in this paper is the stress detection problem, which only focuses on predicting a target user's stress state at once and disregards the continuity of the target user's stress states. In this section, we review related works about stress detection in terms of the following three aspects.

### A. Stress Detection Based on Physical Signals

Some early studies proposed detecting human stress based on physical signals using various machine learning methods. For example, using a set of body language features automatically extracted from visual cues collected by a camera as the inputs, Aigrain et al. [38] applied a support vector machine (SVM) to perform stress detection. As another case, a stress detection framework is proposed in [39], which digests video recordings of human facial cues and utilizes five machine learning classification algorithms to achieve satisfactory detection accuracy. While the study in [39] was also built on multimodal features, such as eye-related events, oral activity, and head movements, only the most robust feature was selected for detection, while the information contained in other multimodal features was disregarded. Baltaci and Gokcay [28] fully emphasized the importance of fusing multimodal features for stress detection. However, in [28], the authors fused pupil dilation and facial thermal change features based on a simple concatenation operation.

Recent works from various domains have demonstrated the power of deep learning in improving the accuracy of classification tasks. Thus, many physical signal-based studies have proposed stress detection methods based on deep learning techniques. For example, Zhang et al. [40] presented a connected convolutional network to predict human stress, which is trained via three facial expressions associated with stress, i.e., anger, fear, and sadness. As another example, in [41], a new CNN-based stress detection architecture is designed, which is trained based on the collected computer records, facial expressions, body postures, and other data of different subjects collected by the camera and wearable devices. Although the authors in [40], [41] propose to utilize multimodal data, they directly connect the multimodal data in the data preprocessing phase, which will result in the formation of high-dimensional feature spaces without proper fusion and may lead to greater computational and storage resources being needed.

### B. Stress Detection Based on Physiological Signals

Previous studies have shown that analyzing physiological signals is a reliable means of detecting human stress [12], [25]. Many good stress detection methods have been proposed based on the collection and analysis of physiological signals.

Mozos et al. [42] propose to combine two sensor systems that separately capture physiological and social responses to detect stress of people in social situations, and the discriminant ability of each sensor system for stress detection is carefully evaluated in the study. Rodríguez-Arce et al. [10] used Arduino boards and low-cost sensors to predict the stress of students

in an academic environment. Although the detection in this study relies on the respiratory rate, heart rate, skin temperature, and blood oxygen data of students, it has two limitations: 1) only the most robust physiological feature is ultimately used for detection and 2) inconvenient wearable devices are used to collect students' physiological signals. Halim and Rehan [43] presented a machine learning approach to identify driving-induced stress patterns, in which ongoing brain activity is logged as an EEG signal to determine the link between brain dynamics and stress states. Salankar et al. [9] presented an effective method using MLP and SVM to identify stress markers via the frontal, temporal, central, and occipital lobes. Specifically, a variational mode decomposition strategy is used to preprocess multimodal physiological signals, which slightly ensures the quality of the extracted physiological signals. Al-Shorman et al. [8] used frontal EEG spectral analysis to detect stress, where the fast Fourier transform (FFT) was applied in the feature extraction stage, while SVM and Naive Bayes classifiers were chosen for stress detection. This approach does not use raw or unprocessed data, which allows for more accurate utilization of physiological signal features and, as a result, guarantees the detection performance of its model.

The idea of deep learning has also recently been used to enhance stress detection performance based on physiological signals. First, Masood and Alghamdi [15] proposed employing two wearable devices to monitor people's physiological signals (e.g., heart rate and breathing) and then applying multiple convolutional layers and recurrent neural networks (RNNs) with long short-term memory (LSTM) layers to detect their stress states. Although this study extracts the brain features from the neural signals to enrich its modality information, those multimodal signals are simply concatenated as model inputs, which disregards the correlation among the features, further causing the features of some modes to contribute less to the final result or to be obscured after the concatenation. Yu and Sano [14] built a stress detection model trained by passive perception data from wearable sensors, mobile phones, and weather APIs. When abundant modalities serve as input, the model itself is a combination of CNN and LSTM models, which do not properly employ multimodal data and may cause the introduction of irrelevant or redundant information, even amplifying the effect of noise and affecting the robustness and performance of the model. In [13], Li and Liu proposed a CNN-based solution that analyzes physiological data collected from a sensor worn on the chest of a person to detect his or her stress states. This solution also combines multimodal features by concatenating them. The work presented in [44] presented a new stress model, which relies on a sequential neural network model to predict human stress. The proposed model preprocesses physiological data collected by wearable devices through the RNN pipeline.

Although existing physiological signal-based methods have shown effectiveness in detecting human stress, most of them rely on wearable sensor devices to collect physiological signals, which are not user friendly. On the other hand, these methods fail to utilize effectively the collected multimodal physiological signals when designing their detection frameworks, while we argue that correlations between different

TABLE I  
DIFFERENCES BETWEEN THE PROPOSED DST METHOD AND RELATED HUMAN STRESS DETECTION METHODS

Methods	Relying on what to detect human stress			How to detect human stress			
	Physiological signals	Non-contact sensor	Multimodal data	Continuous tracing	Feature fusion	Information exchange among multimodal data	Deep learning
SD_HCI [28]	✗	✗	✓	✗	✓	✗	✓
SD_FC [39]	✗	✓	✗	✗	✗	✗	✗
SD_WPSS [42]	✓	✗	✓	✗	✗	✗	✗
PSNS [15]	✓	✗	✓	✗	✗	✗	✓
SD_AE [10]	✓	✗	✓	✗	✗	✗	✗
DeepCNN [13]	✓	✗	✓	✗	✓	✗	✓
RTEEG [8]	✓	✗	✗	✗	✗	✗	✗
Mostress [44]	✓	✗	✗	✗	✓	✗	✓
IEBDNN [41]	✓	✗	✗	✗	✓	✗	✓
WiStress [30]	✓	✓	✗	✗	✓	✗	✓
mmStress [31]	✗	✓	✓	✓	✓	✗	✓
<b>DST (Ours)</b>	✓	✓	✓	✓	✓	✓	✓

modalities of physiological signal data cannot be sufficiently exploited via a simple fusion operation.

### C. Stress Detection Based on Wireless Sensing

In recent years, wireless sensing technology has rapidly developed due to its high sensing accuracy and ability to protect privacy and support many applications, such as hand pose estimation [33], human activity recognition [34], [45], and autonomous driving [46], [47]. In recent years, few works have been proposed to handle human stress detection tasks via wireless signals. In [30], WiStress is presented to detect human stress states based on the analysis of physiological signals collected by a contactless mmWave radar. Specifically, WiStress sends mmWave signals to a target user, analyzes the signals reflected by the user to derive his or her heartbeat, and then infers the user's stress states. Then, mmStress [31] was proposed to detect human stress on the basis of displacement activities related to human stress (i.e., activities generally displayed by a user under stress, such as walking around, scratching, and stomping), which are extracted from mmWave signals. WiStress and mmStress have provided solutions for detecting human stress in a noncontact manner. However, these two methods either only employ uni-modal signals [30] or fail to exchange information among multimodal data and thus cannot effectively fuse and utilize multimodal signals from target users [31] to optimize stress detection tasks, which results in unsatisfactory detection results.

In view of the limitations of related works, this paper gathers multimodal physiological signals via noncontact UWB radar and applying the idea of information exchange [48] to allow information from different modalities to be more effectively exchanged, fused, and utilized. Thus, our proposal, i.e., the DST method, outperforms existing methods and has better generalization in handling different multimodal datasets. Although we propose applying UWB radar rather than mmWave radar in our problem setting, the proposed DST method can also be applied to execute stress tracing tasks based on mmWave radar after simple adaptation. Table I compares the research gaps between the proposed DST method and related methods, showing the advantages of DST.

## III. PRELIMINARIES

In this section, first, we introduce the background of RF-based physiological signal (i.e., HR and RR) sensing with signal modeling. Second, we formally define the concept of stress tracing and then elaborate on the stress tracing problem using UWB radar, which is analyzed in this paper.

**Background.** The rationale of RF-based physiological signal sensing is that a tiny shift in the chest wall caused by physiological movements (i.e., heartbeat and breathing) changes the propagation distance of the reflected RF signal and thus changes the phase of the received RF signal from which we can extract physiological signals. To collect periodically changing physiological signals using UWB radar, the radar sends frames at regular intervals and superimposes the received frames to form the channel impulse response (CIR) matrix. Let  $\mathbf{R} = \{\mathbf{r}_1, \mathbf{r}_2, \dots, \mathbf{r}_t, \dots\}$  be a sequence of a target user's CIR matrices.  $\mathbf{r}_t \in \mathbf{R}$  is in the form of  $\mathbf{r}_t = [r_t^1, \dots, r_t^n, \dots, r_t^N]^T$ , the channel impulse response (CIR) matrix received by a UWB radar, where  $t$  and  $n$  are the *fast-time* index and *slow-time* index, respectively, and  $N$  is the number of slow-time frames [49]. Each row of the CIR matrix (denoted as  $r_t^n$ ) represents the signal received by the radar after sending one frame of signals, while each column of the CIR matrix denotes the change in time over a certain distance of the reflected signal. By modulating the phase from the received CIR matrices and extracting the frequency component, we can extract the HR and RR signals.

**Definition III.1. Stress tracing.** Given continuous observations of physical or physiological signals that can reflect the stress state of the target user, the aim of stress tracing is to continuously monitor changes in the user's stress state. The output of a stress tracing task for a target user is a time series of stress states in the form of  $S = \{s_1, s_2, \dots, s_t, \dots\}$ , where  $s_t \in \{0, 1\}$  denotes the predicted stress state of the user w.r.t. the  $t^{\text{th}}$  time step and  $s_t = 1$  indicates that the user is under stress, while  $s_t = 0$  signals that the user is not under stress. According to the definition of stress categories based on the ground truth of the samples in the dataset, the task target can be changed from a two-category prediction task to a multi-category prediction task.

**Definition III.2. Stress tracing problem using UWB radar.**

Let  $\mathbf{X} = \{\mathbf{x}_1, \mathbf{x}_2, \dots, \mathbf{x}_t, \dots\}$  be a sequence of a target user's physiological signals extracted by a sequence of this target user's CIR matrices  $\mathbf{R} = \{\mathbf{r}_1, \mathbf{r}_2, \dots, \mathbf{r}_t, \dots\}$  collected via a UWB radar.  $\mathbf{x}_t \in \mathbf{X}$  is in the form of  $\mathbf{x}_t = \{\mathbf{hr}_t, \mathbf{rr}_t, \mathbf{RF}_t\}$ , which contains three modalities, namely,  $\mathbf{hr}_t$  (heart rate signal),  $\mathbf{rr}_t$  (respiratory signal), and  $\mathbf{RF}_t$  (RF embedding), all of which are extracted from the raw RF signal  $\mathbf{r}_t$  of the UWB radar at time step  $t$ . The objective of the stress tracing problem using UWB radar is to continuously predict and output the stress state of the target user for every time step based on  $\mathbf{X}$ , i.e., to derive  $S = \{s_1, s_2, \dots, s_t, \dots\}$ , where  $s_t \in S$  is the predicted stress state for the time step  $t$ .

#### IV. DST METHOD

In this section, we outline the architecture of the proposed DST method and then elaborate on each component implemented in DST.

##### A. Overview

Overall, DST has a multimodal architecture that digests three signal modalities, i.e., heart rate (HR), respiratory rate (RR), and RF embedding (RF) extracted from the raw RF signals of a UWB radar to trace the stress states of target users. Figure 2 depicts the network architecture of the proposed DST method, which mainly has three modules, namely, *signal extraction module (SEM)*, *multimodal fusion module (MFM)*, and *stress tracing module (STM)*. First, SEM is responsible for extracting reliable HR and RR signals from the raw RF data collected by a UWB radar. It is noteworthy that the CNN layer and self-attentive mechanism are applied in SEM to address two challenges facing signal extraction, namely non-linearity of signals [50] and unintentional body movements of target users [51]. Second, MFM is in charge of computing robust fused representations of three modalities. In specific, inspired by the idea of coarse-fine-grained parallel feature fusion proposed in [52] and [53], the information from the fine-grained modalities (i.e., HR and RR) are exchanged with the coarse-grained modality (i.e., RF embedding) at different stages via a mechanism of cross connections [54] in MFM, so that the semantic gap among different modalities can be narrowed [55], [56] during the computation of the fused representations of three modalities. Apparently, the proposed MFM makes DST not only strengthen the relationship between coarse-grained (global) features and fine-grained (local) features, but also compensate for the differences in different modalities, to guarantee information from different modalities can be effectively fused and utilized. Last, STM models the temporal dynamics and capture the sequential relationships in the continuous stream of those fused representations of three modalities outputted by MFM, which enables a better learning of the evolution of a target user's stress states within the stream and thereby facilitates the tracing of his or her stress states.

Next, we elaborate on the implementation details of every module in the proposed DST method.

##### B. Signal Extraction Module

The signal extraction module (SEM) targets the extraction of reliable HR and RR signals from the raw RF data collected by a UWB radar with the two challenges facing signal extraction, i.e., non-linearity of signals [50] and unintentional body movements of the target user [51]. The implementation details of the SEM are displayed in Figure 2. First, the background noise is removed from the raw RF data by the mean difference of the signal technique, which is a commonly used, simple but effective signal preprocessing method in the wireless signal processing domain [57], [58]. Second, a fast Fourier transform (FFT) is applied to convert the time domain signal (denoted by the matrix  $\mathbf{X}^T \in \mathbb{R}^{L \times M}$ ) of the RF data in which background noise has been filtered out into the frequency domain signal (denoted by the matrix  $\mathbf{X}^F \in \mathbb{R}^{L \times N}$ ). Here,  $L$  is the cardinality of continuous time frames in sample data, and  $M$ ,  $N$  are the number of time samples and the number of spectral samples respectively in a time frame. Then, three stacked layers, i.e., the CNN layer, self-attention layer, and extraction layer, are successively used to process the derived time domain inputs and frequency domain inputs. In the following section, we separately explain the implementation of the three layers.

1) *CNN Layer*: The CNN layer in the SEM adopts the typical two-stream scheme [59] to process the derived time domain input  $\mathbf{X}^T$  and frequency domain input  $\mathbf{X}^F$  in parallel. Note that  $\mathbf{X}^T$  (or  $\mathbf{X}^F$ ) contains a series of continuous time frames of signals in the time domain (or frequency domain). With  $\mathbf{X}^T$  and  $\mathbf{X}^F$  as the inputs, a one-dimensional CNN is separately applied to  $\mathbf{X}^T$  and  $\mathbf{X}^F$  to extract the periodic variations from the time domain  $\mathbf{X}^T$  (represented as a matrix  $\mathbf{X}^{T_v} \in \mathbb{R}^{L \times C}$  with  $C$  being the number of output channels in the CNN layer) and the condensed spectral peaks from the frequency domain  $\mathbf{X}^F$  (denoted by the matrix  $\mathbf{X}^{F_p} \in \mathbb{R}^{L \times C'}$  with  $C'$  being the number of output channels in the CNN layer), respectively.  $\mathbf{X}^{T_v}$  and  $\mathbf{X}^{F_p}$  indicate the existence of HR and RR signals in the RF data. Then, the concatenation of  $\mathbf{X}^{T_v}$  and  $\mathbf{X}^{F_p}$ , i.e.,  $\mathbf{X}^{TF} = \mathbf{X}^{T_v} \oplus \mathbf{X}^{F_p} \in \mathbb{R}^{L \times (C+C')}$ , which encodes the information of both the time domain and the frequency domain, is fed into the following self-attention layer for further processing.

2) *Self-attention Layer*: Note that the physiological HR and RR signals of the target user change over time and display the internal temporal correlation within the observation sequence of HR and RR. In view of this, a multi-head self-attention mechanism [60] is applied in the attention layer to capture the temporal correlation among the time frames in  $\mathbf{X}^{TF}$ , which is output by the previous CNN layer and encodes the information from both time domain and frequency domain. Specifically, we apply an  $h$ -head attention mechanism. The encoded matrix of  $\mathbf{X}^{TF} \in \mathbb{R}^{L \times (C+C')}$  after the multi-head attention, denoted as  $\hat{\mathbf{X}}^{TF} \in \mathbb{R}^{L \times (C+C')}$ , is computed by:

$$\begin{aligned} \hat{\mathbf{X}}^{TF} &= \text{MultiHead}(\mathbf{X}^{TF}) \\ &= (\text{head}_1 \oplus \text{head}_2 \dots \oplus \text{head}_h) \mathbf{W}^O, \end{aligned} \quad (1)$$

where  $\text{head}_i = \text{Attention}(\mathbf{x}^{TF}_{W_i^Q}, \mathbf{x}^{TF}_{W_i^K}, \mathbf{x}^{TF}_{W_i^V})$ ,

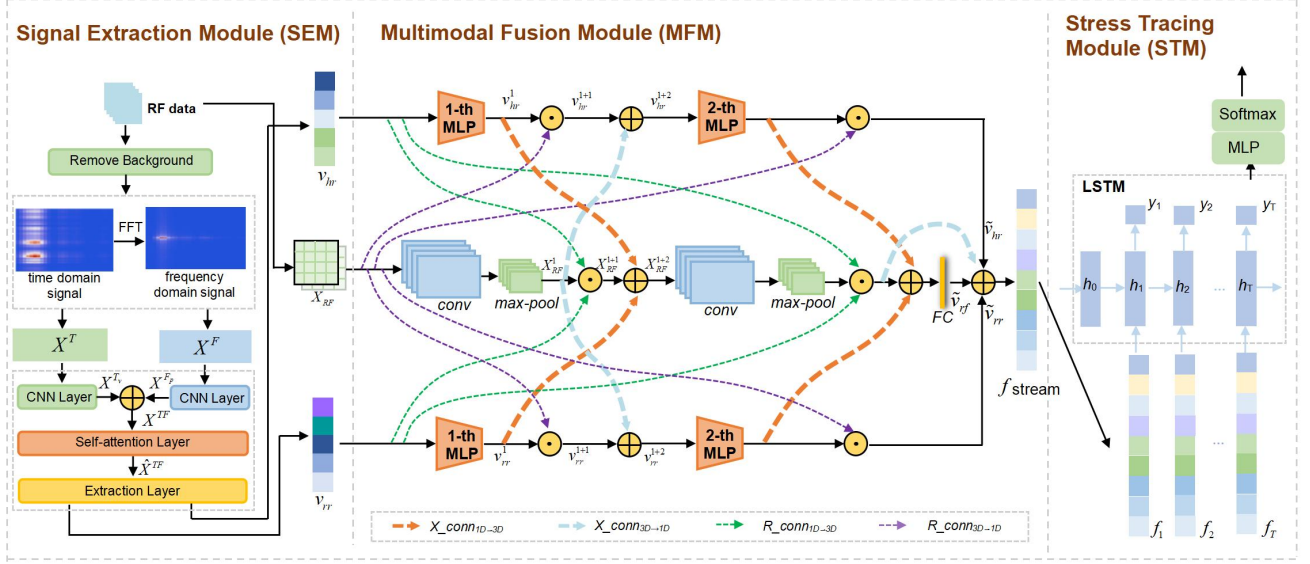


Fig. 2. Architecture of the DST method. The cross connection and residual connection in MFM are represented by  $X_{conn}$  and  $R_{conn}$ , respectively. The former is illustrated by a thick dashed line, while the latter is illustrated by a thin dashed line.  $\odot$  denotes the element-wise addition operation, and  $\oplus$  is the concatenation operation.

where  $h$  represents the number of heads,  $W^O \in \mathbb{R}^{h \times d_k \times (C+C')}$  denotes the weight matrix of the output linear transformation with  $d_k = \frac{1}{h}(C + C')$ ,  $W_i^Q, W_i^K, W_i^V \in \mathbb{R}^{(C+C') \times d_k}$  are learnable projection matrices for the  $i^{th}$  head corresponding to the query, key, and value, respectively.

3) *Extraction Layer*: In the extraction layer, the representations of physiological signals HR and RR are extracted from the outputted matrix of the previous self-attention layer, i.e.,  $\hat{X}^{TF} \in \mathbb{R}^{L \times (C+C')}$ , which encodes the information from the time domain and the frequency domain. The extraction layer performs an average pooling operation toward  $\hat{X}^{TF}$  to aggregate the information of each row in the matrix, which derives an  $L$ -dimensional aggregation vector, denoted as  $v_{tf} \in \mathbb{R}^L$ . Then, the extraction layer, which is a MLP network is used to learn the representations of the HR and RR in parallel. Specifically, the computation of the representation of HR (denoted as  $v_{hr} \in \mathbb{R}^{d_{hr}}$ ) and the representation of RR (denoted as  $v_{rr} \in \mathbb{R}^{d_{rr}}$ ) follows Equation 2.

$$v_{hr} = \text{ReLU}(FC(v_{tf})) = \text{ReLU}(v_{tf}W_{hr} + b_{hr}) \quad (2a)$$

$$v_{rr} = \text{ReLU}(FC(v_{tf})) = \text{ReLU}(v_{tf}W_{rr} + b_{rr}), \quad (2b)$$

where  $W_{hr} \in \mathbb{R}^{L \times d_{hr}}$  and  $W_{rr} \in \mathbb{R}^{L \times d_{rr}}$  are weight matrices,  $b_{hr}$  and  $b_{rr}$  are bias terms, and ReLU is a rectified linear unit activation function.

In summary, the proposed signal extraction module (SEM) in the DST method can extract the representations of HR and RR signals in a robust way. On the one hand, the SEM applies a CNN layer, which enables learning of the nonlinear relationship between HR signals and RR signals in the time domain (or frequency domain). Thus, the SEM can adequately handle the first challenge of non-linearity of signals, which is mentioned at the beginning of Section IV-B.

On the other hand, the self-attention mechanism used in SEM can capture the temporal correlations among the time frames of the received RF data, which is very helpful in decreasing the negative impact of the second challenge, i.e., unintentional body movements of the target user.

### C. Multimodal Fusion Module

As shown in Figure 2, the multimodal fusion module (MFM) effectively fuses three physiological signal modalities of the target user by considering the information exchange among these modalities to ensure that the information from all modalities can be fully utilized in the follow-up stress prediction procedure.

The representations of HR (i.e.,  $v_{hr} \in \mathbb{R}^{d_{hr}}$ ) and RR ( $v_{rr} \in \mathbb{R}^{d_{rr}}$ ) outputted by the previous SEM become the first two modalities digested by the MFM, while RF embedding is the last modality consumed by the MFM. Here, RF embedding is a complementary feature that combines the real part feature of the raw RF data, which reflects the signal strength information, and the imaginary part feature, which contains the signal phase information. Specifically, the RF embedding is represented as a matrix  $X_{RF} \in \mathbb{R}^{L \times M \times 2}$ , and it has two channels: a real part matrix  $X^r \in \mathbb{R}^{L \times M}$  and an imaginary part matrix  $X^i \in \mathbb{R}^{L \times M}$ . We introduce RF embedding as the third processing modality in the MFM due to the rich information that it contains (i.e., HR, RR, head movement, and body posture of the target user), which is very helpful in improving the performance of stress tracing.

Overall, the MFM employs an  $MLP \times CNN \times MLP$  structure to learn a high-quality fusion representation of the three modalities of physiological signals by effectively exchanging information between different modalities. In particular, cross connections and residual connections are concurrently employed in the MFM to implement the information exchange



between the HR (or RR) stream and the RF embedding stream when fusing those three modalities of signals. Both the cross connections and the residual connections can facilitate the learning of cross-modal representations in a neural network layer, i.e., they match the shape of multimodal data to pass the information from one modality to another modality in an end-to-end learnable fashion. In the MFM, both the cross connection and the residual connection are applied multiple times at different processing stages of the MFM to ensure adequate information exchange between signal streams of different modalities. Next, we introduce cross connections and residual connections in detail.

1) *Cross Connection*: As shown in Figure 2, a cross connection is illustrated by a thick dashed line in the MFM, which exchanges information across different modalities of signals. Specifically, cross connections focus on performing the information exchange between the intermediate representations of two signal streams having different modalities at each processing stage of the MFM. During an information exchange procedure, the exchanged information from one stream is fused with the intermediate representation of the other stream. Note that different modalities of signals generally have different dimensions. Such as an HR (or RR) observation is represented as a 1D vector, while an RF embedding is a 3D vector. Due to the fundamental incompatibility between 1D data and 3D data, as shown in Figure 2, the intermediate representation of the HR (or RR) stream learned by a MLP layer cannot be directly delivered and fused with the intermediate representation of the RF embedding stream, which is learned by a {conv, max-pool} block, and vice versa. Therefore, more complicated implementation of cross connections is required to enable information exchange between different modalities of signals in a sensible manner and to allow useful interpretations of these transfers. Thus, in the MFM, we propose two types of cross connections, namely, 3D→1D cross connection and 1D→3D cross connection to execute the information exchange between signal streams of HR (or RR) and RF embedding.

The 3D→1D cross connection (denoted as  $X_{conn3D \rightarrow 1D}$ ), which is illustrated as a thick blue dashed line in Figure 2, is designed to pass the information contained in the RF embedding stream to the HR (or RR) stream, whose structure is demonstrated in the upper half of Figure 3. As shown in the figure, using the output of the  $i^{th}$  {conv, max-pool} block (denoted as  $X_{RF}^i$ ) in the CNN as the input,  $X_{conn3D \rightarrow 1D}$  processes the input via a 2D convolutional layer. The processing result is then flattened and processed by a fully connected layer, whose result is concatenated with the intermediate representation of HR (or RR) (denoted as  $v_{hr}^i, v_{rr}^i$ ), and the result of the 3D→1D cross connection is presented as  $v_{hr}^{i+2}$  (or  $v_{rr}^{i+2}$ ).

The 1D→3D cross connection (denoted by  $X_{conn1D \rightarrow 3D}$ ), which is represented by an orange thick dashed line in Figure 2, is responsible for transferring the information contained in the HR (or RR) stream to the RF embedding stream. The implementation details of  $X_{conn1D \rightarrow 3D}$  are provided in the lower part of Figure 3. As shown in the figure,  $v_{hr}^i$  (or  $v_{rr}^i$ ) acts as the input of  $X_{conn1D \rightarrow 3D}$ . Note that  $v_{hr}^i$  (or  $v_{rr}^i$ ) represents the intermediate representation of the

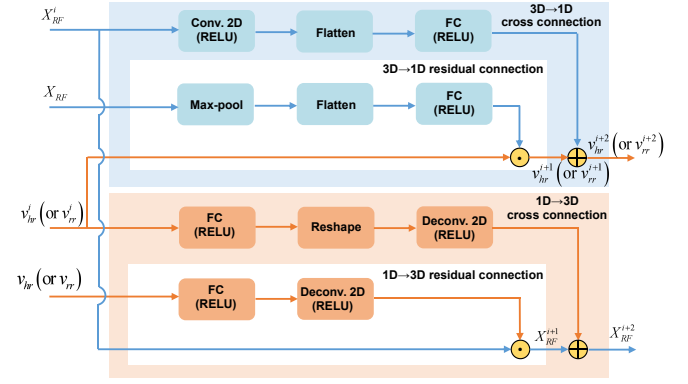


Fig. 3. Architecture of each type of cross connection embedded with a residual connection

HR (or RR) outputted by the  $i^{th}$  MLP layer in the MFM, which is displayed in Figure 2.  $X_{conn1D \rightarrow 3D}$  processes the input by a fully connected layer, and the processing result is then reshaped and processed by a 2D deconvolution layer that converts the 1D representation of the signal to its 3D representation during the training process. The output of the 2D deconvolution layer is concatenated with  $X_{RF}^i$ , i.e., the intermediate representation of RF embedding outputted by the  $i^{th}$  {conv, max-pool} block, to obtain the result of the 1D→3D cross connection (presented as  $X_{RF}^{i+2}$ ).

2) *Residual Connection*: As displayed in Figure 2, a residual connection is denoted by a thin dashed line in the MFM. The residual connection is the process of directly adding inputs to the output of the network layer in residual learning to ensure that the information can be more precisely passed and updated in the network [61]. The purpose of introducing the residual connection into the MFM is to ensure that the representation of HR, RR, or RF embedding extracted by the signal extraction module (i.e.,  $v_{hr}, v_{rr}, X_{RF}$ ) can precisely exchange its information with the intermediate representation of another modality computed by each processing stage in the MFM. Figure 3 also illustrates the architecture of the two types of residual connections proposed in the MFM: 1D→3D residual connection (denoted by  $R_{conn1D \rightarrow 3D}$ ) and 3D→1D residual connection (denoted by  $R_{conn3D \rightarrow 1D}$ ). Specifically,  $R_{conn3D \rightarrow 1D}$  processes the input  $v_{rf}$  through a max-pooling layer. The processing result is then flattened and processed by a fully connected layer, whose result is added with the intermediate representation of HR (or RR) (i.e.,  $v_{hr}^i, v_{rr}^i$ ) by an element-wise addition operation. The addition result is the output of the 3D→1D residual connection, which is represented as  $v_{hr}^{i+1}$  (or  $v_{rr}^{i+1}$ ). Different from  $R_{conn3D \rightarrow 1D}$ ,  $R_{conn1D \rightarrow 3D}$  uses  $v_{hr}$  (or  $v_{rr}$ ) as the input, which is then successively processed by a fully connected layer and a 2D deconvolution layer, the output of the 2D deconvolution layer is added with the intermediate representation of RF embedding (i.e.,  $X_{RF}^i$ ) to form the final output result of the 1D→3D residual connection, which is denoted as  $X_{RF}^{i+1}$ .

As shown in Figure 3, a residual connection is straightforwardly embedded into its counterpart cross connection. Such

an architecture that concurrently applies cross connections and residual connections to achieve information exchange among streams of different modalities provides the potential benefit of correcting unwanted impacts that may be caused by information exchange. For example, to pass information from the HR stream to the RF embedding stream, the 1D→3D cross connection embedded with a residual connection is employed, which uses  $v_{hr}^i$  (i.e., the output of the  $i^{th}$  MLP layer that processes HR in the MFM) and  $v_{hr}$  as the inputs and outputs the new intermediate representation of RF embedding encoding the HR information, which is denoted as  $X_{RF}^{i+2}$  and computed via Equations 3-4.

$$X_{RF}^{i+1} = X_{RF}^i + (W_{v_{hr}v_{hr}} + b_{v_{hr}}) * K_{v_{hr}} \quad (3)$$

$$X_{RF}^{i+2} = X_{RF}^{i+1} \oplus \text{Reshape} \left( W_{v_{hr}^i v_{hr}^i} + b_{v_{hr}^i} \right) * K_{v_{hr}^i}, \quad (4)$$

where  $W_{v_{hr}}$ ,  $W_{v_{hr}^i}$ ,  $K_{v_{hr}}$  and  $K_{v_{hr}^i}$  are learnable weights,  $b_{v_{hr}}$  and  $b_{v_{hr}^i}$  are learnable biases.

Note that the cross connection embedded with a residual connection is used in each processing stage of the MFM to enhance the information exchange between different modalities of signals. As shown in Figure 2, in the MFM, the final representation of every modality of signal (i.e.,  $\tilde{v}_{hr}$ ,  $\tilde{v}_{rr}$ , or  $\tilde{v}_{rf}$ ), which absorbs the information from other modalities of signals, is concatenated. The concatenation result  $\mathbf{f} = \tilde{v}_{rr} \oplus \tilde{v}_{hr} \oplus \tilde{v}_{rf} \in \mathbb{R}^{d_f}$  is the learned fusion representation of three modalities of signals which is outputted by the MFM and then used by the following stress tracing module (STM) to predict the stress state of the target user.

#### D. Stress Tracing Module

Using  $\mathbf{f}_t$ , i.e., the fusion representation of multimodal physiological signals of the target user at a certain time step  $t$ , as the input, the stress tracing module (STM) is used to predict the stress state of the target user at the time step. As shown in Figure 2,  $\mathbf{f}_t$  is fed to an LSTM layer as the  $t^{th}$  element of the  $\mathbf{f}$  stream in the STM, and the LSTM layer is responsible for effectively learning the long-term dependencies within the  $\mathbf{f}$  stream to better predict the stress states of the target user. Specifically, the output of the LSTM layer in the form of  $\mathbf{o}_t$  is defined by:

$$\begin{aligned} \mathbf{o}_t &= f_o(\mathbf{h}_t), \\ \text{where } \mathbf{h}_t &= f_h(\mathbf{f}_t, \mathbf{h}_{t-1}), \end{aligned} \quad (5)$$

where  $\mathbf{h}_0 \in \{0\}^{d_h}$ , and  $f_h$ ,  $f_o$  are a state transition function and an output function, respectively.

Then, the output of the LSTM layer  $\mathbf{o}_t$  at time step  $t$  is passed to a fully connected layer and a softmax activation in the STM to obtain  $y_t$ , which denotes the predicted probability that the target user is under stress at time step  $t$ . Specifically,  $y_t$  is computed by:

$$y_t = \text{softmax}(\mathbf{W}_{o_t} \mathbf{o}_t + \mathbf{b}_{o_t}), \quad (6)$$

where  $\mathbf{W}_{o_t} \in \mathbb{R}^{h \times d}$  is the learnable weight matrix,  $\mathbf{b}_{o_t}$  is the learnable bias. In the training phase, the average loss is computed by the binary cross-entropy, which is defined as follows:

$$L = \frac{1}{N} \sum_{n=1}^N \sum_{t=0}^{T^n} \hat{y}_t^n \log y_t^n + (1 - \hat{y}_t^n) \log (1 - y_t^n), \quad (7)$$

where  $N$  is the cardinality of the  $\mathbf{f}$  stream and  $T^n$  is the latest time step in the  $\mathbf{f}$  stream.  $y_t^n$  is the predicted probability that the target user is under stress at time step  $t$ , and  $\hat{y}_t^n \in \{0, 1\}$  is the ground-truth label of the stress state of the target user at time step  $t$ .

## V. EXPERIMENTS

### A. Stress-inducing Protocol

Determining whether a target user is under stress based on physiological signals is a non-trivial task since we must ensure that the changes in measured physiological signals are caused by human stress and not by other factors such as emotions, physical activity, and environmental factors. Inspired by related studies [8], [13], [15], we propose inducing stress by presenting known stress activities to the target user. In particular, we design a stress-inducing protocol to ensure that the physiological signals used for predicting the stress states of the target user are collected when the target user is under stress. The stress-inducing protocol contains three types of tasks, namely, the neutral task, non-stress task, and stress task, which we describe below.

- **Neutral task.** The neutral task is similar to the anticipation period task in [62]. In this task, a target user is required to sit and answer simple questions such as "How are you feeling?" and "How are you doing today?". The goal of the task is to allow the target user to rest between different types of tasks.
- **Non-stress task.** In the non-stress task, the target user is asked to listen to instrumental music while the user is seated and as relaxed as possible. Sometimes, for certain individuals, a task that induces stress may paradoxically be more relaxing than a task without stress. To address this issue, the target user is instructed to close their eyes, imagine relaxing scenery, and minimize any thoughts of tension to enhance the state of relaxation. For instance, research [63] indicates that closing one's eyes while listening to music can alleviate stress.
- **Stress task.** Previous works [62], [64] have shown that a question-and-answer task with a time limit may induce stress in the target user. In [15], the stress-inducing protocol used multiple stress tasks to ensure that participants felt stressed while they were performing these stress tasks. In our setting, the target user is asked to complete a Stroop color-word interference test (**stress task A**) and a mental math test (**stress task B**), which are widely used stress tasks in stress detection, in a limited amount of time. Specifically, the stress task A requires the target user to select the color of the word



while that word expressed literally is printed in a different color. When handling stress task A, the target user's stress is caused by the contradiction between verbal perception and visual perception. In contrast to stress task A, stress task B induces stress in the target user by asking the user to choose the correct option for the computation of a particular value. Note that the negative feedback (i.e., "Wrong answer!" or "Too slow!") was displayed to the target user to strengthen the stress induction in stress task A or B if the answer given by the user was incorrect or not submitted within the limited time. Moreover, the remaining time for answering each question is marked with a countdown, and the question-answering interface is displayed with different colors of flashing borders (i.e., green, orange, and red) at different time points when answering the question to ensure the effectiveness of stress induction. To further stimulate the stress of the target user, within a stress task, the user is given either a candy (correct answer) or an electrical stimulation (incorrect answer) according to his or her question-answering performance. According to a study [65], expose to electrical stimulation causes fear, whereas the anticipation of electrical stimulation causes stress. In this study, electrical stimulation consisted of a brief pulse with a duration of 500 ms and a current of less than 5.0 mA (mild stimulating sensation without pain). Notably, it is the content and setting of the task rather than the length of the task that causes stress for the target user.

To demonstrate the effectiveness of the proposed stress-inducing protocol, we used the *Depression Anxiety Stress Scales* with 42-questions (DASS-42) after the target user completed the experiment. Specifically, the DASS-42 consists of three subscales, namely, *Stress*, *Anxiety*, and *Depression*, with a total of 42 questions. The three subscales of the DASS-42 examine the degree to which the target user experiences stress, anxiety, and depression. In our setting, only the *Stress* subscale in the DASS-42 is considered due to the topic discussed in this study, where the higher the score given by the target user is, the greater the stress state of the user. The contents of the *Stress* subscale of the DASS-42 are shown in Figure 4.

## B. Experimental Setup

1) *Dataset Collection*: To collect the dataset that contains multimodal signals captured by a UWB radar, we designed a data collection activity based on the proposed stress-inducing protocol in Section V-A. Table II shows demographics of all target users (i.e., participants) involved in our experiments. All participants reported normal vision and hearing and none of them reported taking any medication or receiving any medication or psychological treatment. Specifically, the procedure of the data collection activity contains three sessions, which are illustrated in Figure 5 and elaborated below.

- **Familiarization Session**: As shown in Figure 5, in the familiarization session, the purpose and procedure of the data collection activity are explained to each participant.

DASS-42 of Stress				
Please read each statement and circle a number 0,1,2 or 3 which indicates how much the statement applied to you felt in the experiment. There are no right or wrong answers. Do not spend too much time on any statement.				
The rating score is as follows:				
0 Did not apply to me at all.				
1 Applied to me to some degree, or some of the time				
2 Applied to me to a considerable degree, or a good part of time				
3 Applied to me very much, or most of the time				
1. I found myself getting upset by quite trivial things.	0	1	2	3
2. I tended to over-react to situations.	0	1	2	3
3. I found it difficult to relax.	0	1	2	3
4. I found myself getting upset rather easily.	0	1	2	3
5. I felt that I was using a lot of nervous energy.	0	1	2	3
6. I found myself getting impatient when I was delayed in any way (eg. elevators, traffic lights, being kept waiting).	0	1	2	3
7. I felt that I was rather touchy.	0	1	2	3
8. I found it hard to wind down.	0	1	2	3
9. I found that I was very irritable.	0	1	2	3
10. I found it hard to calm down after something upset me.	0	1	2	3
11. I found it difficult to tolerate interruptions to what I was doing	0	1	2	3
12. I was in a state of nervous tension.	0	1	2	3
13. I was intolerant of anything that kept me from getting on with what I was doing.	0	1	2	3
14. I found myself getting agitated.	0	1	2	3

Fig. 4. Stress subscale of the DASS-42

TABLE II  
DEMOGRAPHICS OF TARGET USERS INVOLVED IN EXPERIMENTS

Demographics	Information
Gender	6 females, 11 males
Age	17 to 30 years
Height	153 to 187 cm
Weight	44 to 91 kg
Occupation	Various industries
Health background	Healthy

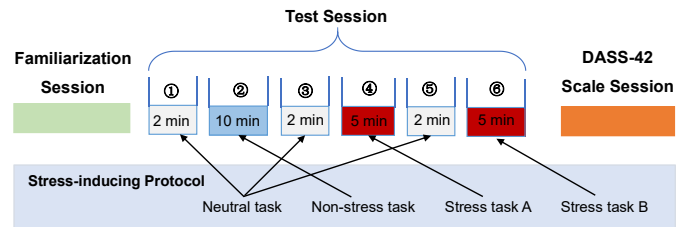
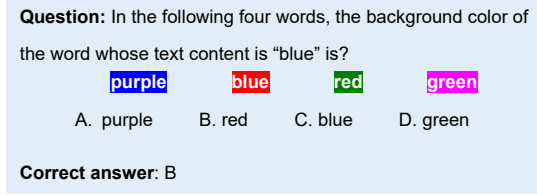


Fig. 5. The data collection procedure was based on a stress-inducing protocol (min: minutes)

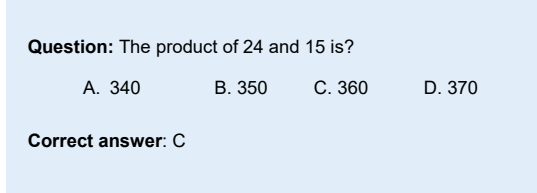
Since each task in the proposed stress-inducing protocol (i.e., neutral task, non-stress task, or stress task) is assigned to the participants in an online test system, the participants are given a short demonstration to understand how to perform each task. Note that the order and duration of each task are the same for each participant. The participants are informed that a UWB radar is used in the activity to collect their physiological data. At the end of the familiarization session, a UWB radar sensor is

placed on a table in front of each participant, after which a one-minute data acquisition test is conducted to verify proper operation of the data collection function of the UWB radar.

- **Test Session:** Figure 5 shows that the test session involves a sequence of tasks, including the neutral task, non-stress task and stress task, which are defined in the stress-inducing protocol. Specifically, this session starts with a neutral task that lasts two minutes, which is followed by a non-stress task that lasts 10 minutes. Afterward, the neutral task (lasting 2 minutes) and each stress task (lasting 5 minutes) appeared alternately in the session. As previously mentioned, each participant was supposed to correctly answer as many questions as possible in the time allotted to them during the stress task. Figure 6a and Figure 6b show an example question set for task A and task B in our experiment, respectively. The ground-truth labels of the stress state of the target user in stress task A and stress task B are labeled as 1 (indicating under stress), while the ground-truth labels of the stress state of the target user in the non-stress task are labeled as 0 (indicating no stress).



(a) An example of question in stress task A



(b) An example of question in stress task B

Fig. 6. Examples of questions in the stress tasks

- **DASS-42 Scale Session:** To verify the effectiveness of the proposed stress-inducing protocol, the DASS-42 scale was used for the data collection activity. The DASS-42 consists of 42 questions, and each participant is only asked to complete the *Stress* subscale of the DASS-42, which contains 14 questions with a 4-point Likert scale. The higher the score on the stress subscale of the DASS-42 is, the greater the stress level of the target user. In addition, we evaluated the effectiveness of the stress-inducing protocol by analyzing the average and standard deviation of the target users' scores on each item of the stress subscale of the DASS-42.

Figure 7 shows a real-world scene of the data collection activity, where the target user works on a stress task and the UWB radar that is placed in front of the user continuously collects the user's multimodal physiological signal data. To obtain the multimodal dataset collected by the UWB radar, 17 target

TABLE III  
DESCRIPTION OF THE THREE MULTIMODAL DATASETS (N=RESPIBAN, E=EMPATICA E4, AND R=UWB RADAR)

Name	Target users	classes	Samples	Sensors
WESAD <sup>2</sup>	15	2	31082	N, E
WESAD <sup>3</sup>	15	3	66304	N, E
Self-Collected	17	2	60992	R

users are invited to participate into the study. Specifically, there are 6 female target users and 11 male target users, ranging in age from 17 to 30 years. Each participant is required to act as the target user and complete the experiment according to the experiment settings, and the experiment is completed once in each of the three scenarios (i.e., classroom, conference room, and bedroom).

2) **Datasets:** We evaluated the performance of DST using the two publicly available datasets most frequently used in stress detection tasks and a new multimodal stress detection dataset that we collected in the real-world. Table III shows the descriptions of the three datasets. The WESAD dataset [66] is the most frequently employed dataset in the field of stress detection and can be used to evaluate the performance of a model. According to the setting of stress categories, the WESAD dataset includes the two-category WESAD<sup>2</sup> dataset and the three-category WESAD<sup>3</sup> dataset. Compared to these two datasets, our dataset provides richer information of modalities using both physiological signals and physical signals. Furthermore, unlike the above two datasets collected via wearable sensors, our dataset uses a contactless sensor (i.e., UWB radar), which is more friendly to the target user and does not cause possible interference to the target user's stress state.

**WESAD<sup>2</sup> dataset** [66]. This dataset contains multimodal physiological data collected from 15 target users which are collected by two human wearable sensors. It can be used for the binary (i.e., stress and non-stress) stress detection task. Specifically, a RespiBAN sensor is used to collect the data which has a sampling rate of 700Hz and 8 sensing channels, while another sensor used for collecting data, i.e., Empatica E4, has a sampling rate of 64Hz and 6 sensing channels. In our experiment, we choose a 1-second wide time window to generate a feature matrix based on the data collected by each sensor and deem those data generated by a different sensor are data from different modality. We use the data collected from 12 target users for training a human stress detection model and employ the remaining data collected from the other 3 target users for testing the performance of the model in handling stress tracing tasks.

**WESAD<sup>3</sup> dataset** [66]. The WESAD<sup>3</sup> dataset follows most of the settings of the WESAD<sup>2</sup> dataset. Being different from the WESAD<sup>2</sup> dataset, each sample in the WESAD<sup>3</sup> dataset is labeled with a more detailed stress state (i.e., baseline, stress, and amusement), rather than only two categories of stress states (i.e., stress and non-stress) used by the WESAD<sup>2</sup> dataset. Therefore, the WESAD<sup>3</sup> dataset can be used to evaluate the performance of different stress detection models in distinguishing more stress categories.

**Self-collected dataset.** It is a self-collected real-world dataset which is derived following the stress-inducing protocol proposed in Section V-A. Specifically, this dataset contains multi-modal physiological signals of 17 target users (11 males and 6 females) collected by a UWB radar deployed in three different indoor environments, including classroom, conference room, and bedroom. A typical scene for data collection is shown in Figure 7. We choose a 5-second wide sliding time window to collect RF data and each sample in the dataset is labeled with a binary stress state, where 1 indicates under stress and 0 represents non-stress. Specifically, the self-collected data contains two modalities of data, namely heart rate (HR) and respiratory rate (RR). We use the data collected from 14 target users for training a human stress detection model and employ the remaining data collected from the other 3 target users for testing the performance of different models in handling a stress tracing task.

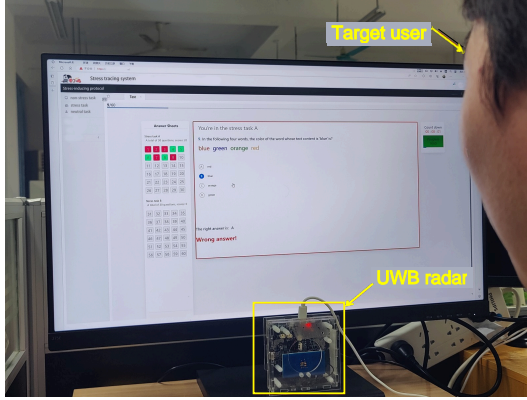


Fig. 7. A real-world scene of the data collection activity

3) *Baselines*: The effectiveness of the proposed DST method is compared with that of ten baselines, all of which are vital physiological-based methods for human stress detection. We list all comparison baselines and their descriptions below.

- **SD\_AE** [10]: it proposes to use the physiological features to predict human stress in an academic environment. Specifically, SD\_AE employs the  $k$ -nearest neighbor algorithm to select the most robust physiological feature and uses it for predicting human stress states.
- **RTEEG** [8]: it utilizes the features extracted from a single physiological signal via the Fast Fourier Transform as the input, and employs the support vector machine for human stress detection.
- **PSNS** [15]: it concatenates multiple physiological signals from two modalities through the mathematical pre-processing, and then uses multiple convolutional layers and recurrent neural networks (RNN) with LSTM layers to detect stress of the target user.
- **DeepCNN** [13]: it extracts features from multiple physiological signals using a 1D-CNN and treats the concatenation of all feature vectors as its input. Then, multiple fully connected layers are utilized in DeepCNN to achieve the prediction of human stress states.
- **Mostress** [44]: it uses a time-series-based RNN structure to achieve the stress detection. Note that Mostress makes

use of the mathematical computations on the physiological data collected by wearable devices to improve the performance of stress detection.

- **IEBDNN** [41]: it simply connects various physiological signals to get the fusion feature in the pre-processing stage, and then encodes those fusion features into GAF images which are used to train a CNN model for human stress detection.
- **WiStress** [30]: it proposes using the uni-modal physiological signal of a target user, which is collected by an mmWave radar, to achieve the goal of human stress detection. WiStress sends mmWave signals to a target user, analyzes the signals reflected by the user to estimate his or her heartbeat, and infers the user's stress state based on the heartbeat information.
- **mmStress** [31]: it is the latest method for stress detection based on wireless sensing. mmStress predicts human stress by recognizing and analyzing displacement activities under stress (e.g., walking around and scratching) at macro- and micro-temporal scales via a customized neural network.
- **WiStress+SEM**: it is a variant of WiStress where the proposed SEM in DST is used as its signal extraction module.
- **mmStress+SEM**: it is a variant of mmStress where the proposed SEM is used as its signal extraction module.

4) *Evaluation Metrics*: As to the domain of human stress detection, the most commonly used evaluation metrics are accuracy (ACC), F1 score, and area under the curve (AUC). Here, ACC is defined as the proportion of samples with correct predictions over all samples, F1 score is a statistical metric used to measure the accuracy of a binary classification model, and AUC is defined as the area enclosed by the ROC curve and the lower coordinate axis. Generally speaking, the value 0.5 for AUC or ACC indicates that the classification (or detection) performance is the same as the random guessing, and the value 1 for AUC or ACC signals that the detection model achieves perfect performance. Note that the AUC generally takes a value from the range of  $[0, 1]$  and the closer the AUC value is to 1, the better the stress detection performance is. F1 score considers both the precision and recall of the classification model, and it offers a balanced assessment towards a detection model's performance in classifying positive samples and negative samples. For each method, we repeat the training process five times and report the average ACC, F1 score, and AUC in the following experiments.

5) *Radar Selection*: Advantages and disadvantages of two representative types of radars (i.e., FMCW radar and UWB radar) for vital signs detection tasks are usually compared by researchers [67]. Resorting to the power of wide-band, both of the FMCW radar and UWB radar achieve good detection performance due to their high time resolution. However, the UWB radar slightly outperforms FMCW radar since it: i) has fewer harmonics and a higher signal-to-noise ratio (SNR) [67]; ii) is immune to multipath distortions due to its characteristics of short pulse signals [68] while the FMCW radar is susceptible to jamming in the presence of multipath propagation [69]. Another popular type of radar is the millimeter-Wave radar

TABLE IV  
IMPLEMENTATION DETAILS OF MULTIMODAL FUSION MODULE (MFM) IN THE PROPOSED DST METHOD (PARAMETERS OF CROSS CONNECTIONS ARE SHOWN IN **BOLD**,  $\searrow$  DENOTES 1D $\rightarrow$ 3D CROSS CONNECTION, AND  $\swarrow$  DENOTES 3D $\rightarrow$ 1D CROSS CONNECTION).

HR signal stream	RR signal stream	RF embedding stream	Output size
Fully-connected 32D	Fully-connected 32D	Conv. 2D [3 $\times$ 3, 8] Max-pool. [2 $\times$ 2]	((150 $\times$ 96, 8], 32) ((75 $\times$ 48, 8], 32)
<b>Fully-connected 192D</b> <b>Deconv. 2D [16 <math>\times</math> 12, 8]</b> $\searrow$	<b>Fully-connected 192D</b> <b>Deconv. 2D [16 <math>\times</math> 12, 8]</b> $\searrow$	<b>Conv. 2D [1 <math>\times</math> 1, 8]</b> $\swarrow$ <b>Fully-connected 32D</b>	((75 $\times$ 48, 16], 96)
Fully-connected 64D	Fully-connected 64D	Conv. 2D [3 $\times$ 3, 24] Max-pool. [2 $\times$ 2]	((75 $\times$ 48, 24], 64) ((37 $\times$ 24, 24], 64)
<b>Fully-connected 40D</b> <b>Deconv. 2D [8 <math>\times</math> 5, 24]</b> $\searrow$	<b>Fully-connected 40D</b> $\swarrow$ <b>Deconv. 2D [8 <math>\times</math> 5, 24]</b>	<b>Conv. 2D [1 <math>\times</math> 1, 24]</b> $\swarrow$ <b>Fully-connected 64D</b>	((37 $\times$ 24, 72], 192)
Fully-connected 192D			(192, 64)

(mmWave). We do not choose the mmWave radar in our study to collect physiological signals of target users for the following two reasons. First, the mmWave radar is sensitive to the influence of air humidity conditions. In specific, under the condition of a high atmospheric humidity, the transmitted signal of mmWave radar is easy to be scattered and absorbed, which reduces the detection and ranging ability of the mmWave radar [70]. In contrast, the UWB radar maintains a good performance under most conditions of air humidity. Second, the mmWave radar has a lower bandwidth and SNR compared to the UWB radar, which makes it have a relatively weak anti-jamming ability than the UWB radar [67]. It is also noteworthy that due to the wide frequency spectrum distribution of UWB signals that occupies a large frequency range, the UWB radar has a superior immunity to on-air interference from other wireless devices operating in the same frequency band [71] [72]. In other words, the UWB radar can coexist with other communication systems, e.g., Wi-Fi and Bluetooth, without causing significant interference, making it a reliable and robust choice for even those applications that require uninterrupted operations. It is those above-mentioned advantages of the UWB radar that make us select the UWB radar as the basic support for implementing our proposed stress tracing method.

6) *Scenario Settings*: To ensure the UWB radar can effectively detect the stress states of each target user, we require that: i) the position of the target user is within the Field of View (FoV) of the UWB radar so that the radar can receive the reflected signal from the target user, ii) the distance between the radar and the user (i.e., monitoring distance) lies within a reasonable sensing range (generally 0.3 m to 3 m [73]) to alleviate the multipath effect of the UWB radar, and iii) only the body movements that away from the user's chest (e.g., typewriting, limb position drift, drinking water, and yawning) rather than those movements drastically changing the user's posture (e.g., from sitting to lying) are allowed to ensure the monitoring of respiration and heart rate of the user is not affected.

7) *Other Settings*: For the signal extraction module (SEM) in the proposed DST method, the dimensionality of each of the two fully connected layers in the self-attention layer of SEM is set to 64 to facilitate the signal extraction. Note that the *ReLU* activation function is applied to all convolutional and fully-connected layers in DST. The multimodal fusion

module (MFM) is the most complicated module in DST, since different modalities of signals and their interactions are processed and learned in the module. Table IV summarizes the implementation details of MFM, where the description of residual connections in MFM is omitted for they can be inferred from the shape of the output. To combat overfitting, a couple of regularization techniques are employed in MFM. Specifically, the batch normalization technique is applied after the input layer (or the operation that fuses  $\tilde{v}_{hr}$ ,  $\tilde{v}_{rr}$ , and  $\tilde{v}_{rf}$ ) in MFM, which normalizes the input to each layer, reduces internal covariate shift, and improves model generalization. Besides, the dropout technique is applied after every max-pooling layer in MFM with a dropout rate of 0.25. Notice that a larger dropout rate of 0.5 is applied after the first fully-connected layer in MFM. This is because the fully-connected layer has more parameters than each of the max-pooling layers and a larger dropout rate offers more help to counteract overfitting for the fully-connected layer. For the stress tracing module (STM) in DST, the size of the hidden layer of the LSTM is set to 64, and the LSTM layer is followed by a fully-connected layer with a 2-way softmax activation function for stress tracing. It is worth noting that the dropout rate in the LSTM layer is set to 0.25.

To evaluate each comparison model, 80% of the collected dataset are used as the training set and the remaining 20% are treated as the test set. During the training stage of every model, we use Adam with a batch size of 40, and run the experiments with 50 epochs, while the learning rate is set to 0.001 for all comparison methods. We use a commercial off-the-shelf UWB radar from AIWise [74] to collect experimental data. The radar operates at 7.3 GHz with a bandwidth of 1.4 GHz and 150 frames per second (FPS); it has a pair of Tx-Rx antennas with a field of view of 65° angle. In addition, all comparison methods are implemented by PyTorch 2.1, and trained using the same hyper-parameters on a Linux server with an Intel Core i9-11900 CPU (8 cores), a NVIDIA RTX A5000 GPU, and 128 GB DDR4 RAM. To ensure the fairness of comparison, all baselines compared in the following experiments are tuned to their best performance.

### C. Experimental Analysis

1) *Hyper-parameter sensitivity*: In this section, we provide a sensitivity analysis for two hyper-parameters which are used by the proposed DST method.

- **Impact of the number of convolutional layers in the CNN layer of SEM.** Figure 8a displays the impact of different number of convolutional layers in the CNN layer of SEM (denoted as  $N_{CNN}$ ) on the performance of DST on the self-collected dataset, when the number of heads set for the self-attention mechanism in SEM of DST (denoted as  $N_{head}$ ) is fixed to 4. As shown in the figure, with the increase of  $N_{CNN}$ , the value of ACC, F1 score, or AUC displays a gradual downward trend. This may be because each convolutional layer transforms the information, and as the number of convolutional layers increases, the time-domain and frequency-domain information in the input data will gradually be lost, making DST be unable to effectively capture important features in the input data. Thus,  $N_{CNN}$  is set to 1 in DST on self-collected dataset in the following experiments, to ensure that DST achieves best performance. On WESAD<sup>2</sup> and WESAD<sup>3</sup> datasets, CNNs are used to encode features from the inputted multimodal data. Figures 8b and 8c show the impact of different  $N_{CNN}$  on the two datasets separately, when  $N_{head}$  is fixed to 4. As shown by the two figures, DST consistently gains its best performance when  $N_{CNN}$  equals to 3, due to the over-fitting phenomena. Therefore,  $N_{CNN}$  is set to 3 on the WESAD<sup>2</sup> and WESAD<sup>3</sup> datasets in the following experiments.

- **Impact of the number of heads in SEM.** Figures 9 investigates the impact of different amount of head (i.e.,  $N_{head}$ ) set for the self-attention mechanism in SEM on the prediction performance of DST on three datasets, while the number of convolutional layers  $N_{CNN}$  is fixed to 1. As demonstrated by these three figures, when  $N_{head}$  equals to 4, DST achieves its best performance in terms of ACC, F1 score, and AUC, while introducing more heads beyond 4 degrades the performance of DST. Therefore,  $N_{head}$  is set to 4 in the following experiment in DST on all datasets in the following experiments, to ensure DST can derive its best prediction results.

2) *Comparison with Baselines:* Table V displays the experimental results of comparing our proposal (i.e., DST) with baselines. Overall, the average improvements in terms of the ACC, F1, and AUC of DST compared with those of best baselines on three datasets are 6.31%, 7.24%, and 6.69%, respectively. DST significantly outperforms all baselines in terms of ACC, F1, and AUC, which demonstrates the superiority of the proposed DST method in extracting and utilizing the multimodal physiological signals of target users when tracing their stress states. Note that two variants of WiStress and mmStress, i.e., WiStress+SEM and mmStress+SEM, are only evaluated on the self-collected dataset, since the embedded SEM in these two variants is designed for extracting HR or RR signals from the raw RF data collected by a UWB radar while the HR or RR data have already been provided in the WESAD<sup>2</sup> or WESAD<sup>3</sup> dataset. Next, we provide a detailed analysis of the results shown in Table V. Specifically, by observing the table, we derive the following findings.

- **Finding 1:** *Deep learning based methods obtain the most accurate stress detection result.* As shown in Table V,

methods that use the traditional machine learning strategies (i.e., SD\_AE and RTEEG) are beaten by those deep learning based methods (i.e., PSNS, DeepCNN, Mostress, IEBDNN, WiStress, mmStress, WiStress+SEM, mmStress+SEM, and DST). This is because deep learning based methods own significant advantages in learning high-quality representations of multimodal physiological signals and they thus can effectively capture the nonlinear relationships between multimodal signals and a target user's stress states.

- **Finding 2:** *Raw physiological signal data need to be processed before they can be used to tracing human stress.* As displayed in Table V, on all datasets, methods that use the processed physiological signal data (i.e., RTEEG, DeepCNN, Mostress, IEBDNN, WiStress, mmStress, WiStress+SEM, mmStress+SEM, and DST) are consistently superior to those methods that directly use the raw physiological signal data (i.e., SD\_AE and PSNS) in detecting human stress. This is because the collected raw physiological signal data generally contain noises from background or unconscious body movements, which brings negative impact on the precision stress detection results. This finding verifies the importance of filtering out the noises in the raw physiological signal data when designing a stress method. First, in DST, the background noise is removed from the raw RF data by mean difference of the signal technique. Second, FFT is applied to convert the time domain signal of the RF data where background noise has been filtered out into the frequency domain signal. Furthermore, the signal extraction module (SEM) of DST can extract the reliable HR and RR signals from the raw RF data collected by a UWB radar addressing the two challenges facing by signal extraction, i.e., non-linearity of signals and unintentional body movements of the target user.
- **Finding 3:** *Optimizing the signal extraction strategy is vital for ensuring the performance of stress detection.* When extracting representations for physiological signals of different modalities, the characteristics of different modalities should be considered. However, many baselines simply apply the same mathematical calculation method (i.e., Mostress and IEBDNN) or the same convolutional network structure (i.e., DeepCNN and PSNS) to learn the representations for physiological signals of different modalities, leading to weak generalization ability, low interpretability, and unsatisfactory stress detection performance. Compared with those baselines, in DST an effective signal extraction module (SEM) is applied. Specifically, in SEM, for the two modalities HR and RR, both of a CNN structure and a multi-head attention mechanism are used to extract their representations which reflect the information of time domain, frequency domain, and temporal correlation within each physiological signal stream. Moreover, to derive a high-quality representation of the third modality in DST (i.e., RF embedding), DST proposes to combine the raw RF data's real part feature which reflects the signal strength information and the imaginary part feature that contains the signal phase



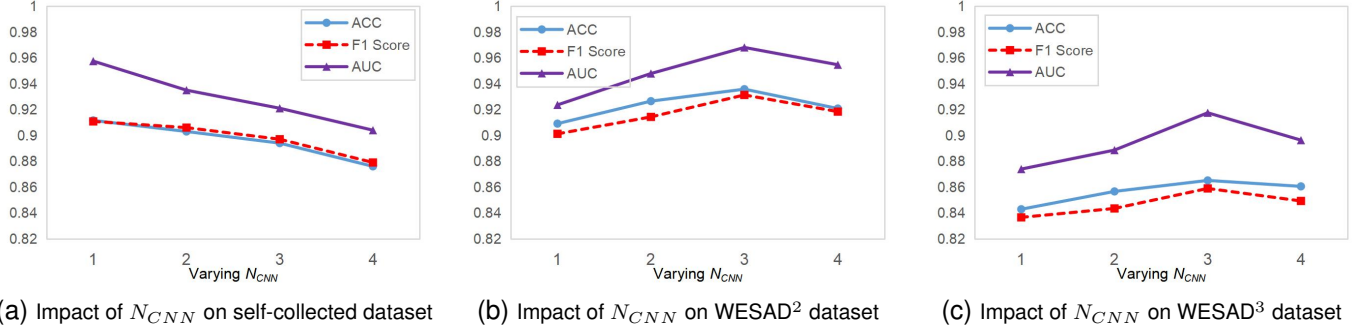


Fig. 8. Sensitivity analysis of the number of convolutional layers ( $N_{CNN}$ ) on three datasets

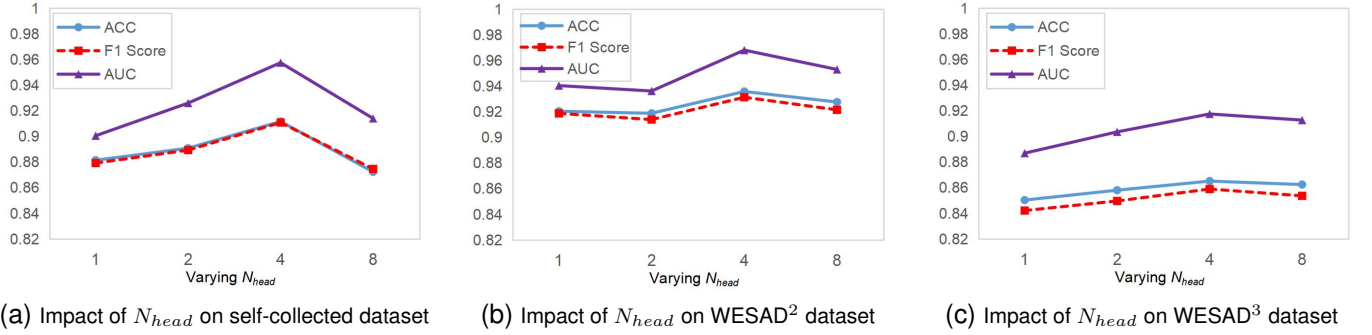


Fig. 9. Sensitivity analysis of the number of heads in self-attention ( $N_{head}$ ) on three datasets

TABLE V

A COMPARISON BETWEEN DST AND BASELINES. DATA MARKED WITH \* DENOTE THE NEXT BEST RESULTS. THE LAST COLUMN GIVES THE IMPROVEMENT RATE GAINED BY DSTS COMPARED WITH THE NEXT BEST RESULTS.

Model	WESAD <sup>2</sup> Dataset			WESAD <sup>3</sup> Dataset			Self-collected Dataset		
	Accuracy (%)	AUC (%)	F1-score (%)	Accuracy (%)	AUC (%)	F1-score (%)	Accuracy (%)	AUC (%)	F1-score (%)
SD_AE [10]	72.87	76.43	72.12	64.35	67.04	63.56	66.77	71.04	64.37
RTEEG [8]	70.63	72.15	70.54	63.69	64.40	63.17	69.29	74.25	68.81
PSNS [15]	80.71	84.18	80.36	73.17	77.03	72.46	72.14	76.47	70.01
DeepCNN [13]	86.35	89.07	85.44	75.32	79.84	74.95	73.15	78.30	73.17
Mostress [44]	81.54	84.91	80.23	74.58	78.16	72.91	73.35	79.78	74.69
IEBDNN [41]	84.32	88.68	84.15	78.43	81.57	77.64	75.59	78.85	73.42
WiStress [30]	83.46	86.72	83.21	77.62	81.73	77.08	84.83	88.36	83.24
mmStress [31]	86.59*	89.57*	86.37*	79.19*	83.28*	78.41*	80.79	85.02	79.53
WiStress+SEM	—	—	—	—	—	—	85.61	88.75	84.41
mmStress+SEM	—	—	—	—	—	—	86.53*	89.72*	85.26*
<b>DST (Ours)</b>	<b>93.58</b>	<b>96.81</b>	<b>93.13</b>	<b>86.51</b>	<b>91.75</b>	<b>85.89</b>	<b>91.16</b>	<b>95.75</b>	<b>91.08</b>
Improvement	6.99	7.24	6.76	7.32	8.47	7.48	4.63	6.03	5.82

information. As shown in Table V, on three datasets, the values of ACC, AUC, and F1 score of DST gain averagely 12.95%, 13.37%, and 13.16% increase separately, compared with Mostress, IEBDNN, DeepCNN, and PSNS which only use less-satisfactory strategies to extract signals. Notice that the effectiveness of the proposed signal extraction strategy (i.e., SEM) in DST can be also verified by comparing WiStress and mmStress with their variants, i.e., WiStress+SEM and mmStress+SEM. In particular, with the application of SEM, these two methods averagely gain performance increase of 0.78% and 5.74% respectively on ACC on the self-collected dataset.

• **Finding 4:** Considering temporal correlation of physiological signals can significantly improve the detection performance. As shown in Table V, DST, mmStress, and mmStress+SEM which can be deemed as the stress tracing methods rather than the stress detection methods perform consistently better than other baselines on all datasets. This is because these three methods consider the temporal correlation of signals derived by applying the self-attention mechanism over each input signal stream. It is the consideration of temporal correlation within a signal stream that makes DST, mmStress, and mmStress+SEM better trace human stress and therefore derive more accurate stress state prediction results.



- **Finding 5:** *Fusing multimodal physiological signals are very important to improve stress detection results.* Fusing multimodal signals aims to learn a stronger representation than via a single modality. In Table V, on all datasets, PSNS that does not utilize the information of multimodal fusion performs worse than other deep learning based baselines that make use of the multimodal information (i.e., DeepCNN, Mostress, IEBDNN, WiStress, mmStress, WiStress+SEM, and mmStress+SEM). Another observation from Table V is that the proposed DST method performs averagely 8.45% and 8.23% better in accuracy compared with WiStress and mmStress separately on all datasets. Notice that WiStress and mmStress are the state-of-the-art non-contact solutions for human stress detection. The superiority of DST comes from the consideration of information exchange among different modalities of sensing signals, while WiStress and mmStress simply concatenate signals of different modalities when training their models.
- **Finding 6:** *DST dramatically outperformed all the baselines.* DST adequately handles the two challenges of extracting physiological signals by considering the information in the time domain and frequency domain of RF signals, and effectively learns the temporal correlation within a single signal via a multi-head self-attention mechanism. Moreover, cross connections with residual connections are used to directly exchange information in the physiological signals of different modalities to better utilize the correlation and complementarity between different modalities, which can improve the ability of DSTs to fuse multimodal signals. Another observation from Table V is that DST performs better on the WESAD<sup>2</sup> dataset than on the other two datasets. On one hand the WESAD<sup>2</sup> dataset is collected by wearable sensors and thus contains relatively less noise than the self-collected dataset, which is collected using non-contact UWB radar. On the other hand, the stress state labels defined on the WESAD<sup>2</sup> dataset only have two categories (i.e., under stress and non-stress), while the stress labels defined on the WESAD<sup>3</sup> dataset have three categories (i.e., baseline, stress, and amusement), which makes the stress tracing task on WESAD<sup>3</sup> dataset more complicated than that on the WESAD<sup>2</sup> dataset.
- **Finding 7:** *DST has a good generalization in handling different sensing data for stress detection.* The significant performance improvement of DST gained on the two publicity datasets (i.e., WESAD<sup>2</sup> and WESAD<sup>3</sup>) compared with baselines also show that DST has a good generalization in handling different multimodal sensing datasets for human stress detection. Notice that both of the WESAD<sup>2</sup> and WESAD<sup>3</sup> datasets are collected through human wearable sensors rather than non-contact radars. The superiority of DST gained on this two datasets, once again, confirms the effectiveness of DST in fusing and utilizing different multimodal sensing data.

we perform an ablation study by comparing DST with its six variants on the self-collected dataset. For a fair comparison, all of the comparison methods are tuned to achieve their best performance. Detailed descriptions of every DST variants are provided below.

- **DST-SEM:** it is a variant of DST that removes the signal extraction module (SEM) and uses a mathematical calculation algorithm [75] to extract HR and RR signals.
- **DST-HR:** it is a variant of DST that eliminates the HR signal stream in Multimodal Fusion Module (MFM).
- **DST-RR:** it is a variant of DST which removes the RR signal stream in MFM.
- **DST-X-R:** it is a variant of DST that cuts off both of the cross connection (i.e.,  $X_{conn}$ ) and residual connection (i.e.,  $R_{conn}$ ) in MFM.
- **DST-RF-X-R:** it is a variant of DST that deletes the RF embedding input of MFM, and removes  $X_{conn}$  and  $R_{conn}$  from MFM.
- **DST-STM:** it is a variant of DST where the Stress Tracing Module (STM) is eliminated and instead a softmax operation is applied by the variant for predicting the human stress states.

Table VI shows the experimental results of the ablation study. First, we notice that DST outperforms every variant of it, which indicates the effectiveness of each modules or inputs designed for DST. Second, the performance of DST-SEM has shown a decrease of 9.8% in ACC, 10.9% in F1 score, and 15.2% in AUC compared with DST. This shows the superiority of the proposed signal extraction module (SEM) in DST towards the mathematical calculation algorithm with respect to extract HR and RR signals from the raw RF data collected by the UWB radar. Specifically, without SEM, it is very difficult for DST-SEM to solve the challenges of signal interference and unintentional body movements when extracting HR and RR signals. Third, since the three variants of DST, namely DST-HR, DST-RR, DST-X-R, and DST-RF-X-R, are derived by revising the implementation of the multimodal fusion module (MFM) in DST, the deteriorating performance of the three variants compared with DST demonstrates the importance of MFM in effectively fusing multimodal physiological signals. In particular, DST-HR and DST-RR perform 2.82% and 2.85% worse in ACC than DST separately, which indicates the vital function of HR or RR physiological signal in tracing the stress state change of a target user. Meanwhile, we can conclude that the proposed cross connection and residual connection in MFM are very important to ensure the adequate information exchange between a pair of signal streams of different modalities, since without using these two types of connections the two related variants of DST, i.e., DST-X-R and DST-RF-X-R, can only generate less satisfactory prediction results. It is the sufficient information exchange among signals of different modalities that makes DST generate high-quality fused representations of multimodal signal data compared with its variants. Notice that DST-X-R retains the RF embedding but achieves worse performance than DST-RF-X-R. Although RF embedding contains richer information than HR or RR signals, it also owns lots of redundant interference information.

3) *Ablation Study:* To analyze the effectiveness of the proposed modules in DST in coping with stress tracing tasks,

TABLE VI  
RESULTS OF ABLATION STUDY ON SELF-COLLECTED DATASET (BEST VALUES ARE IN BOLD)

Metrics	DST-SEM	DST-HR	DST-RR	DST-X-R	DST-RF-X-R	DST-STM	DST
ACC	0.8137	0.8836	0.8831	0.8247	0.8336	0.8710	<b>0.9118</b>
F1 score	0.8019	0.8823	0.8847	0.8239	0.8381	0.8763	<b>0.9108</b>
AUC	0.8055	0.8975	0.9020	0.8385	0.8423	0.8824	<b>0.9575</b>

In such case, when information exchange is not performed in MFM (i.e.,  $X_{conn}$  and  $R_{conn}$  are removed from MFM), introducing the RF embedding stream into MFM (w.r.t. DST-X-R) can only bring negative impact on predicting human stress states. Finally, we can observe from Table VI that DST-STM performs averagely 5.01% worse than DST in terms of all evaluation metrics, which indicates that using the LSTM structure to trace human stress states is more effective than using the simple softmax operation. This is because the LSTM structure is very effective to process time series data and maintain temporal integrity.

4) *Impact of Different Monitoring Distances*: The monitoring distance, i.e., the distance between radar and monitored target user, is a major factor that affects the performance of radar-based applications. To evaluate the impact of different monitoring distances to our proposal, we have set up five scenarios, where the monitoring distance is set to 0.5 m, 1 m, 1.5 m, 2 m, and 2.5 m, separately. In every scenario, a target user is asked to complement three round of experiments according to the stress induction protocol elaborated before, and physiological signal data of the target user in each experiment are collected. Then, the data collected in the first two experiments are used as the training dataset, while the data gathered in the third experiment are treated as the test dataset. Experimental results of the impact of different monitoring distances on the performance of DST are reported in Figure 10a. As shown in the figure, with the increase of the monitoring distance, the ACC (accuracy) of DST gradually declines. In particular, the ACC of DST decreases by 9.91% when distance varies from 0.5 m to 2.5 m. This is because with the increase of monitoring distance: i) the difficulty of the UWB radar to distinguish chest vibrations from other body movements raises; ii) and there is a degradation w.r.t. SNR of the RF signals. In our default experimental settings, the UWB radar is put under the computer display screen (see Figure 7), and thus the monitoring distance generally varies between 0.5 m and 0.6 m, which ensures DST can get its best performance for stress detection tasks. Notice that to ensure the effectiveness of DST in stress tracing (i.e., the stress detection accuracy being larger than 0.9), the maximum monitoring distance is suggested to be 1.5 m.

5) *Impact of Different Radar Placement Angles*: In this section, impact of different radar placement angles (angles for short) on the performance of DST is verified. The radar placement angle demonstrated in Figure 11 is the angle between the radar's normal line and its line pointing to the chest of a target user, and it characterizes a situation of sensor placement (or user face orientation). Specifically, the angle is separately set to 0°, 15°, 30°, 45°, 60° in our experiments reflecting five situations of sensor placement, and the target

user is within the radar field of view (FoV) in all situations. In each situation, the target user is required to complete three round of experiments based on our stress induction protocol, and the RF data gathered in the previous two experiments are used to train DST while the data from the last experiment are applied to test DST. Experimental results of varying angles are displayed in Figure 10b. The figure shows that ACC values for five situations are all above 0.94 and are relatively stable, indicating the robustness of the proposed DST in detecting user stress under the different settings of sensor placement. Meanwhile, Figure 10b also reveals that the performance of DST tenderly increases with the growth of the angle, which is counter-intuitive. This phenomenon can be attributed to the decrease in respiration signal strength with the increase of the angle, which makes the heartbeat signal be less disturbed by the respiration signal [76].

6) *Impact of Different Environmental Conditions*: To show the robustness of DST in handling different environments, we have tested the effectiveness of DST under five environmental conditions, namely E1: classroom, E2: conference room, E3: living room, E4: laboratory, and E5: bedroom. Similarly to Sections V-C4 and V-C5, three round of experiments are performed in every condition and  $\frac{2}{3}$  collected physiological signal data of target user are treated as the training dataset while the remaining  $\frac{1}{3}$  data are used as the test dataset. Experimental results displayed in Figure 10c show that ACC values of the proposed DST method under five environmental conditions are all above 0.9, which indicates the effectiveness of DST in coping with the stress detection problem under different environment settings.

7) *Analysis of DASS-42 Stress Subscale*: In this section, the stress subscale of DASS-42 is used to verify the effectiveness of the stress-inducing protocol proposed in this paper. In Table VII lists the mean ( $M$ ) and standard deviation ( $SD$ ) of the scores given by all target users on the 14 items of the stress subscale. The  $M$  value of each item is basically between 1.5 and 2.3, which indicates that all target users feel a certain degree of stress in the stress task. Table VII also shows that most  $SD$  values are between 0.6 and 1.1, and their variance is within a reasonable range. This means that the scores given by different target users are relatively consistent, which indicates the defined stress-inducing protocol can effectively induce stress for all target users. In DASS-42 Stress Subscale, a total score of all items which is larger than 10 points represents different levels of stress [37]. According to  $M \pm SD$  calculations, the total scores of all items for all target users are all above 10 points, which indicates that each target user has a moderate or higher level of stress when performing the stress task. All analysis results of DASS-42 stress subscale show that the stress task in the proposed stress-

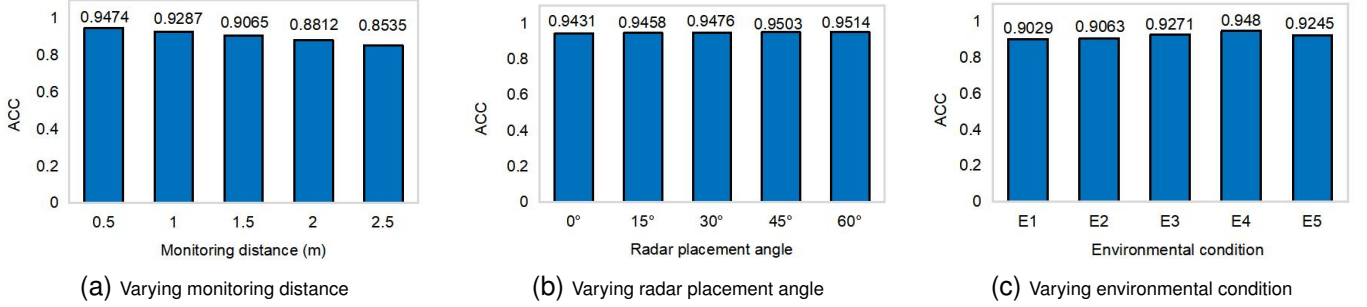


Fig. 10. Performance of DST under different settings

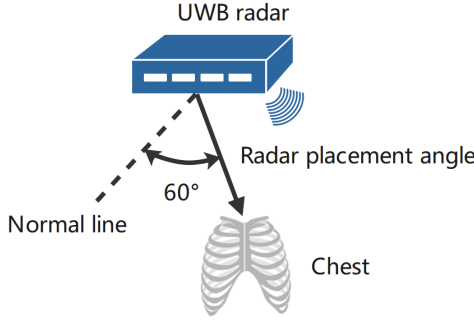


Fig. 11. Illustration of the radar placement angle

TABLE VII  
THE SCORES OF THE PARTICIPANTS ON EACH ITEM ABOUT DASS-42  
STRESS SUBSCALE

Item of question	M $\pm$ SD	Item of question	M $\pm$ SD
S1	2.1 $\pm$ 0.8	S8	2.2 $\pm$ 1.0
S2	1.6 $\pm$ 0.7	S9	1.8 $\pm$ 0.9
S3	1.9 $\pm$ 0.9	S10	1.9 $\pm$ 0.8
S4	2.3 $\pm$ 1.1	S11	2.1 $\pm$ 0.9
S5	1.5 $\pm$ 0.6	S12	1.6 $\pm$ 0.7
S6	2.0 $\pm$ 0.8	S13	1.8 $\pm$ 0.8
S7	1.7 $\pm$ 0.8	S14	2.0 $\pm$ 0.9

inducing protocol can effectively induce stress of target users. This is because both of the questions answered by the target users in a stress task and the target users' anticipation to the arrival of an unknown pulse triggered by wrongly answering a question cause stress.

## VI. CONCLUSION AND FUTURE WORK

In this paper, we formally define the stress tracing problem and present DST, a novel deep network for tracing human stress. Compared with related stress detection methods, DST well solve two vital challenges in stress detection domain, i.e., unfriendly collection of physiological signals from users and failure to effectively utilize multimodal physiological signals. Specifically, unlike most related works that leverage wearable devices to collect physiological signals of users, DST proposes tracing human stress based on physiological signals collected by a contactless UWB radar, which improves user experience. Then, a group of modules, namely, the signal extraction module (SEM) and multimodal fusion module (MFM) are carefully designed in DST to ensure that the multimodal physiological

signals of target users can be effectively extracted, fused, and utilized for tracing their stress states. Experimental results on three real-world datasets demonstrate that DST method delivers significant improvements over state-of-the-art baselines in tracing human stress. One limitation of this study is that we do not consider users' side information and his/her performance when completing the task, which we will consider in the future to identify user stress levels at a finer granularity. For future directions, it is worth exploring how to deploy larger-scale models such as large language models on resource-constrained wearables [77]–[79] and how to collaboratively train models while protecting user privacy [80]–[86].

## ACKNOWLEDGEMENTS

This work is supported by National Natural Science Foundation of China [Nos. 62067001, 62062008].

## REFERENCES

- [1] Shivani Mittal, Sumedha Mahendra, Viraj Sanap, and Prathamesh Churi. How can machine learning be used in stress management: A systematic literature review of applications in workplaces and education. *International Journal of Information Management Data Insights*, 2(2):100110, 2022.
- [2] Zihan Fang, Zheng Lin, Senkang Hu, Hangcheng Cao, Yiqin Deng, Xianhao Chen, and Yuguang Fang. Ic3m: In-car multimodal multi-object monitoring for abnormal status of both driver and passengers. *arXiv preprint arXiv:2410.02592*, 2024.
- [3] Wenning Fu, Chao Wang, Li Zou, Yingying Guo, Zuxun Lu, Shijiao Yan, and Jing Mao. Psychological health, sleep quality, and coping styles to stress facing the covid-19 in wuhan, china. *Translational psychiatry*, 10(1):225, 2020.
- [4] Tianlin Zhang, Kailai Yang, Shaoxiong Ji, and Sophia Ananiadou. Emotion fusion for mental illness detection from social media: A survey. *Information Fusion*, 92:231–246, 2023.
- [5] Giorgos Giannakakis, Dimitris Grigoriadis, Katerina Giannakaki, Olympia Simantiraki, Alexandros Roniotis, and Manolis Tsiknakis. Review on psychological stress detection using biosignals. *IEEE Transactions on Affective Computing*, 13(1):440–460, 2019.
- [6] Yongyang Tang, Zhe Chen, Ang Li, Tianyue Zheng, Zheng Lin, Jia Xu, Pin Lv, Zhe Sun, and Yue Gao. Merit: Multimodal wearable vital sign waveform monitoring. *arXiv preprint arXiv:2410.00392*, 2024.
- [7] Aditi Agarwal, Astha Goel, Shristy Sharma, Soniya Jain, Mani Dwivedi, and Deep Kumar. A novel model for stress detection and management using machine learning. In *2023 International Conference on Disruptive Technologies (ICDT)*, pages 562–570. IEEE, 2023.
- [8] Omar AlShorman, Mahmoud Masadeh, Md Belal Bin Heyat, Faijan Akhtar, Hossam Almahasneh, Ghulam Md Ashraf, and Athanasios Alexiou. Frontal lobe real-time eeg analysis using machine learning techniques for mental stress detection. *Journal of Integrative Neuroscience*, 21(1):20, 2022.

- [9] Nilima Salankar, Deepika Koundal, and Saeed Mian Qaisar. Stress classification by multimodal physiological signals using variational mode decomposition and machine learning. *Journal of Healthcare Engineering*, 2021, 2021.
- [10] Jorge Rodríguez-Arce, Liliana Lara-Flores, Otniel Portillo-Rodríguez, and Rigoberto Martínez-Méndez. Towards an anxiety and stress recognition system for academic environments based on physiological features. *Computer methods and programs in biomedicine*, 190:105408, 2020.
- [11] Yuan Tian. Identification and modeling of college students' psychological stress indicators for deep learning. *Scientific Programming*, 2022:1–9, 2022.
- [12] Shruti Gedam and Sanchita Paul. A review on mental stress detection using wearable sensors and machine learning techniques. *IEEE Access*, 9:84045–84066, 2021.
- [13] Russell Li and Zhandong Liu. Stress detection using deep neural networks. *BMC Medical Informatics and Decision Making*, 20:1–10, 2020.
- [14] Han Yu and Akane Sano. Passive sensor data based future mood, health, and stress prediction: User adaptation using deep learning. In *2020 42nd Annual International Conference of the IEEE Engineering in Medicine & Biology Society (EMBC)*, pages 5884–5887. IEEE, 2020.
- [15] Khalid Masood and Mohammed A Alghamdi. Modeling mental stress using a deep learning framework. *IEEE Access*, 7:68446–68454, 2019.
- [16] Haoxuan Yuan, Zhe Chen, Zheng Lin, Jinbo Peng, Zihan Fang, Yuhang Zhong, Zihang Song, Xiong Wang, and Yue Gao. Graph learning for multi-satellite based spectrum sensing. In *2023 IEEE 23rd International Conference on Communication Technology (ICCT)*, pages 1112–1116, 2023.
- [17] Zheng Lin, Guanqiao Qu, Xianhao Chen, and Kaibin Huang. Split learning in 6g edge networks. *IEEE Wirel. Commun.*, 2024.
- [18] Yongyi Chen, Dan Zhang, Hamid Reza Karimi, Chao Deng, and Wutao Yin. A new deep learning framework based on blood pressure range constraint for continuous cuffless bp estimation. *Neural Networks*, 152:181–190, 2022.
- [19] Zheng Lin, Guanqiao Qu, Qiyuan Chen, Xianhao Chen, Zhe Chen, and Kaibin Huang. Pushing large language models to the 6g edge: Vision, challenges, and opportunities. *arXiv preprint arXiv:2309.16739*, 2023.
- [20] Haoxuan Yuan, Zhe Chen, Zheng Lin, Jinbo Peng, Zihan Fang, Yuhang Zhong, Zihang Song, and Yue Gao. Satsense: Multi-satellite collaborative framework for spectrum sensing. *arXiv preprint arXiv:2405.15542*, 2024.
- [21] Jinbo Peng, Zhe Chen, Zheng Lin, Haoxuan Yuan, Zihan Fang, Lingzhong Bao, Zihang Song, Ying Li, Jing Ren, and Yue Gao. Sums: Sniffing unknown multiband signals under low sampling rates. *arXiv preprint arXiv:2405.15705*, 2024.
- [22] Zhe Chen, Tianyue Zheng, and Jun Luo. Octopus: A practical and versatile wideband mimo sensing platform. In *Proceedings of the 27th Annual International Conference on Mobile Computing and Networking*, pages 601–614, 2021.
- [23] Xingzhe Song, Hongshuai Li, and Wei Gao. Myomonitor: Evaluating muscle fatigue with commodity smartphones. *Smart Health*, 19:100175, 2021.
- [24] Lu Han, Qiang Zhang, Xianxiang Chen, Qingyuan Zhan, Ting Yang, and Zhan Zhao. Detecting work-related stress with a wearable device. *Computers in Industry*, 90:42–49, 2017.
- [25] Jerry Chen, Maysam Abbod, and Jiann-Shing Shieh. Pain and stress detection using wearable sensors and devices—a review. *Sensors*, 21(4):1030, 2021.
- [26] Stephanie Carreiro, Keerthi Kumar Chintha, Sloke Shrestha, Brittany Chapman, David Smelson, and Premananda Indic. Wearable sensor-based detection of stress and craving in patients during treatment for substance use disorder: A mixed methods pilot study. *Drug and alcohol dependence*, 209:107929, 2020.
- [27] Elena Smets, Walter De Raedt, and Chris Van Hoof. Into the wild: the challenges of physiological stress detection in laboratory and ambulatory settings. *IEEE journal of biomedical and health informatics*, 23(2):463–473, 2018.
- [28] Serdar Baltaci and Didem Gokcay. Stress detection in human-computer interaction: Fusion of pupil dilation and facial temperature features. *International Journal of Human-Computer Interaction*, 32(12):956–966, 2016.
- [29] Zheng Lin, Guangyu Zhu, Yiqin Deng, Xianhao Chen, Yue Gao, Kaibin Huang, and Yuguang Fang. Efficient parallel split learning over resource-constrained wireless edge networks. *IEEE Trans. Mob. Comput.*, 2024.
- [30] Unsoo Ha, Sohrab Madani, and Fadel Adib. Wistress: Contactless stress monitoring using wireless signals. *Proceedings of the ACM on Interactive, Mobile, Wearable and Ubiquitous Technologies*, 5(3):1–37, 2021.
- [31] Kun Liang, Anfu Zhou, Zhan Zhang, Hao Zhou, Huadong Ma, and Chenshu Wu. mmstress: Distilling human stress from daily activities via contact-less millimeter-wave sensing. *Proceedings of the ACM on Interactive, Mobile, Wearable and Ubiquitous Technologies*, 7(3):1–36, 2023.
- [32] Shujie Zhang, Tianyue Zheng, Hongbo Wang, Zhe Chen, and Jun Luo. Quantifying the physical separability of rf-based multi-person respiration monitoring via sinr. In *Proceedings of the 20th ACM Conference on Embedded Networked Sensor Systems*, pages 47–60, 2022.
- [33] Jia Xu, Biao Yang, Zhe Chen, Pin Lv, Shujie Zhang, and Jun Luo. Skefit: Estimating hand poses via rf vision under low contrast and occlusion. *IEEE Internet of Things Journal*, 2023.
- [34] Pin Lv, Shuyu Luo, Jia Xu, Zhe Chen, and Heng Liu. Ocro: Open-set cross-domain human activity recognition based on radio frequency. *IEEE Internet of Things Journal*, 2023.
- [35] Degui Yang, Zhengliang Zhu, Junchao Zhang, and Buge Liang. The overview of human localization and vital sign signal measurement using handheld ir-uwv through-wall radar. *Sensors*, 21(2):402, 2021.
- [36] Zongxing Xie, Hanrui Wang, Song Han, Elinor Schoenfeld, and Fan Ye. Deepvs: a deep learning approach for rf-based vital signs sensing. In *Proceedings of the 13th ACM international conference on bioinformatics, computational biology and health informatics*, pages 1–5, 2022.
- [37] Luke Parkitny and James McAuley. The depression anxiety stress scale (dass). *Journal of physiotherapy*, 56(3):204, 2010.
- [38] Jonathan Aigrain, Séverine Dubuisson, Marcin Detyniecki, and Mohamed Chetouani. Person-specific behavioural features for automatic stress detection. In *2015 11th IEEE international conference and workshops on automatic face and gesture recognition (FG)*, volume 3, pages 1–6. IEEE, 2015.
- [39] Giorgos Giannakakis, Matthew Pedititis, Dimitris Manousos, Eleni Kazantzaki, Franco Chiarugi, Panagiotis G Simos, Kostas Marias, and Manolis Tsiknakis. Stress and anxiety detection using facial cues from videos. *Biomedical Signal Processing and Control*, 31:89–101, 2017.
- [40] Jin Zhang, Xue Mei, Huan Liu, Shenqiang Yuan, and Tiancheng Qian. Detecting negative emotional stress based on facial expression in real time. In *2019 IEEE 4th international conference on signal and image processing (ICSIP)*, pages 430–434. IEEE, 2019.
- [41] Sayandeep Ghosh, SeongKi Kim, Muhammad Fazal Ijaz, Pawan Kumar Singh, and Mufti Mahmud. Classification of mental stress from wearable physiological sensors using image-encoding-based deep neural network. *Biosensors*, 12(12):1153, 2022.
- [42] Oscar Martinez Mozos, Virginia Sandulescu, Sally Andrews, David Ellis, Nicola Bellotto, Radu Dobrescu, and Jose Manuel Ferrandez. Stress detection using wearable physiological and sociometric sensors. *International journal of neural systems*, 27(02):1650041, 2017.
- [43] Zahid Halim and Mahma Rehan. On identification of driving-induced stress using electroencephalogram signals: A framework based on wearable safety-critical scheme and machine learning. *Information Fusion*, 53:66–79, 2020.
- [44] Arturo de Souza, Mateus B Melchiades, Sandro J Rigo, and Gabriel de O Ramos. Mostress: A sequence model for stress classification. In *2022 International Joint Conference on Neural Networks (IJCNN)*, pages 1–8. IEEE, 2022.
- [45] Xiaomin Ouyang, Xian Shuai, Jiayu Zhou, Ivy Wang Shi, Zhiyuan Xie, Guoliang Xing, and Jianwei Huang. Cosmo: contrastive fusion learning with small data for multimodal human activity recognition. In *Proceedings of the 28th Annual International Conference on Mobile Computing And Networking*, pages 324–337, 2022.
- [46] Zhiqing Wei, Fengkai Zhang, Shuo Chang, Yangyang Liu, Huici Wu, and Zhiyong Feng. Mmwave radar and vision fusion for object detection in autonomous driving: A review. *Sensors*, 22(7):2542, 2022.
- [47] Ronghui Zhang, Xiaojun Jing, Sheng Wu, Chunxiao Jiang, Junsheng Mu, and F Richard Yu. Device-free wireless sensing for human detection: The deep learning perspective. *IEEE Internet of Things Journal*, 8(4):2517–2539, 2020.
- [48] Syed Waqas Zamir, Aditya Arora, Salman Khan, Munawar Hayat, Fahad Shahbaz Khan, Ming-Hsuan Yang, and Ling Shao. Multi-stage progressive image restoration. In *Proceedings of the IEEE/CVF conference on computer vision and pattern recognition*, pages 14821–14831, 2021.
- [49] Kuo-Kai Shyu, Luan-Jiau Chiu, Po-Lei Lee, Tzu-Han Tung, and Shun-Han Yang. Detection of breathing and heart rates in uwv radar sensor data using fvpief-based two-layer eemd. *IEEE sensors journal*, 19(2):774–784, 2018.

- [50] G Jasmine Christabel and AC Subhajini. Kpca-wrf-prediction of heart rate using deep feature fusion and machine learning classification with tuned weighted hyper-parameter. *Network: Computation in Neural Systems*, pages 1–32, 2023.
- [51] Zongxing Xie, Ava Nederlander, Isac Park, and Fan Ye. Rf-q: Un-supervised signal quality assessment for robust rf-based respiration monitoring. In *2023 IEEE/ACM Conference on Connected Health: Applications, Systems and Engineering Technologies (CHASE)*, pages 158–162. IEEE, 2023.
- [52] Yuxin Peng, Jinwei Qi, Xin Huang, and Yuxin Yuan. Ccl: Cross-modal correlation learning with multigrained fusion by hierarchical network. *IEEE Transactions on Multimedia*, 20(2):405–420, 2017.
- [53] Ming Jin, Huaxiang Zhang, Lei Zhu, Jiande Sun, and Li Liu. Coarse-to-fine dual-level attention for video-text cross modal retrieval. *Knowledge-Based Systems*, 242:108354, 2022.
- [54] Petar Veličković, Duo Wang, Nicholas D Lane, and Pietro Liò. X-cnn: Cross-modal convolutional neural networks for sparse datasets. In *2016 IEEE symposium series on computational intelligence (SSCI)*, pages 1–8. IEEE, 2016.
- [55] Öykü Deniz Köse and Murat Saraçlar. Multimodal representations for synchronized speech and real-time mri video processing. *IEEE/ACM Transactions on Audio, Speech, and Language Processing*, 29:1912–1924, 2021.
- [56] Anubhav Bhatti, Behnam Behinaein, Dirk Rodenburg, Paul Hungler, and Ali Etemad. Attentive cross-modal connections for deep multimodal wearable-based emotion recognition. In *2021 9th international conference on affective computing and intelligent interaction workshops and demos (ACIIW)*, pages 01–05. IEEE, 2021.
- [57] Yuxing Li, Bo Geng, and Bingzhao Tang. Simplified coded dispersion entropy: A nonlinear metric for signal analysis. *Nonlinear Dynamics*, 111(10):9327–9344, 2023.
- [58] Lukáš Klein, David Seidl, Jan Fulneček, Lukáš Prokop, Stanislav Mišák, and Jiří Dvorský. Antenna contactless partial discharges detection in covered conductors using ensemble stacking neural networks. *Expert Systems with Applications*, 213:118910, 2023.
- [59] Fanghui Bi, Tiantian He, Yuetong Xie, and Xin Luo. Two-stream graph convolutional network-incorporated latent feature analysis. *IEEE Transactions on Services Computing*, 2023.
- [60] Ashish Vaswani, Noam Shazeer, Niki Parmar, Jakob Uszkoreit, Llion Jones, Aidan N Gomez, Lukasz Kaiser, and Illia Polosukhin. Attention is all you need. *Advances in neural information processing systems*, 30, 2017.
- [61] Kaiming He, Xiangyu Zhang, Shaoqing Ren, and Jian Sun. Deep residual learning for image recognition. In *Proceedings of the IEEE conference on computer vision and pattern recognition*, pages 770–778, 2016.
- [62] Virginia Sandulescu, Sally Andrews, David Ellis, Nicola Bellotto, and Oscar Martinez Mozos. Stress detection using wearable physiological sensors. In *Artificial Computation in Biology and Medicine: International Work-Conference on the Interplay Between Natural and Artificial Computation, IWINAC 2015, Elche, Spain, June 1-5, 2015, Proceedings, Part I 6*, pages 526–532. Springer, 2015.
- [63] Francisca N Ogbia, Moses O Ede, Charity N Onyishi, Patricia U Agu, Amaka B Ikechukwu-Illomuanya, Janet N Igbo, Nkechi Egenti, Ifeyinwa Manafa, Chijioke Amoke, Nneka C Nwosu, et al. Effectiveness of music therapy with relaxation technique on stress management as measured by perceived stress scale. *Medicine*, 98(15), 2019.
- [64] Mario Salai, István Vassányi, and István Kósa. Stress detection using low cost heart rate sensors. *Journal of healthcare engineering*, 2016, 2016.
- [65] Jamie L Rhudy and Mary W Meagher. Fear and anxiety: divergent effects on human pain thresholds. *Pain*, 84(1):65–75, 2000.
- [66] Philip Schmidt, Attila Reiss, Robert Duerichen, Claus Marberger, and Kristof Van Laerhoven. Introducing wesad, a multimodal dataset for wearable stress and affect detection. In *Proceedings of the 20th ACM international conference on multimodal interaction*, pages 400–408, 2018.
- [67] Dingyang Wang, Sungwon Yoo, and Sung Ho Cho. Experimental comparison of ir-uwv radar and fmcw radar for vital signs. *Sensors*, 20(22):6695, 2020.
- [68] Yanjia Luo and Choi Look Law. Indoor positioning using uwb-ir signals in the presence of dense multipath with path overlapping. *IEEE Transactions on wireless communications*, 11(10):3734–3743, 2012.
- [69] Li Lu, Muhammad Jawad Hussain, and Zhigang Han. A fmcw-based cross layer rf distance bounding scheme. *IEEE Transactions on Wireless Communications*, 15(6):4009–4016, 2016.
- [70] Qinglang Dai, Yongzhi Huang, Lu Wang, Rukhsana Ruby, and Kaishun Wu. mm-humidity: Fine-grained humidity sensing with millimeter wave signals. In *2018 IEEE 24th International Conference on Parallel and Distributed Systems (ICPADS)*, pages 204–211. IEEE, 2018.
- [71] Chutao Zheng, Yuchu Ge, and Anfu Guo. Ultra-wideband technology: Characteristics, applications and challenges, 2023.
- [72] Xiaohao Chen, Maosheng Fu, Zhengyu Liu, Chaochuan Jia, and Yu Liu. Harris hawks optimization algorithm and bp neural network for ultra-wideband indoor positioning. *Mathematical Biosciences and Engineering*, 19(9):9098–9124, 2022.
- [73] Tianyue Zheng, Zhe Chen, Shujie Zhang, Chao Cai, and Jun Luo. More-fi: Motion-robust and fine-grained respiration monitoring via deep-learning uwb radar. In *Proceedings of the 19th ACM conference on embedded networked sensor systems*, pages 111–124, 2021.
- [74] WiRUSH. Aiwise intelligent manufacturing. <https://www.wirush.ai/aiwise>, Mar 2023.
- [75] Xiaolin Liang, Hao Zhang, Shengbo Ye, Guangyou Fang, and T Aaron Gulliver. Improved denoising method for through-wall vital sign detection using uwb impulse radar. *Digital Signal Processing*, 74:72–93, 2018.
- [76] Shujie Zhang, Tianyue Zheng, Zhe Chen, and Jun Luo. Can we obtain fine-grained heartbeat waveform via contact-free rf-sensing? In *IEEE INFOCOM 2022-IEEE conference on computer communications*, pages 1759–1768. IEEE, 2022.
- [77] Zheng Lin, Xuanjie Hu, Yuxin Zhang, Zhe Chen, Zihan Fang, Xianhao Chen, Ang Li, Praneeth Vepakomma, and Yue Gao. Splitlora: A split parameter-efficient fine-tuning framework for large language models. *arXiv preprint arXiv:2407.00952*, 2024.
- [78] Zihan Fang, Zheng Lin, Zhe Chen, Xianhao Chen, Yue Gao, and Yuguang Fang. Automated federated pipeline for parameter-efficient fine-tuning of large language models. *arXiv preprint arXiv:2404.06448*, 2024.
- [79] Yuhang Qiu, Honghui Chen, Xingbo Dong, Zheng Lin, Iman Yi Liao, Massimo Tistarelli, and Zhe Jin. Ifvit: Interpretable fixed-length representation for fingerprint matching via vision transformer. *arXiv preprint arXiv:2404.08237*, 2024.
- [80] Mingda Hu, Jingjing Zhang, Xiong Wang, Shengyun Liu, and Zheng Lin. Accelerating federated learning with model segmentation for edge networks. *IEEE Transactions on Green Communications and Networking*, 2024.
- [81] Zheng Lin, Guanqiao Qu, Wei Wei, Xianhao Chen, and Kin K Leung. Adaptsfl: Adaptive split federated learning in resource-constrained edge networks. *arXiv preprint arXiv:2403.13101*, 2024.
- [82] Yuxin Zhang, Zheng Lin, Zhe Chen, Zihan Fang, Wenjun Zhu, Xianhao Chen, Jin Zhao, and Yue Gao. Satfed: A resource-efficient leo satellite-assisted heterogeneous federated learning framework. *arXiv preprint arXiv:2409.13503*, 2024.
- [83] Tianyue Zheng, Ang Li, Zhe Chen, Hongbo Wang, and Jun Luo. Autofed: Heterogeneity-aware federated multimodal learning for robust autonomous driving. In *Proceedings of the 29th Annual International Conference on Mobile Computing and Networking*, pages 1–15, 2023.
- [84] Yuxin Zhang, Haoyu Chen, Zheng Lin, Zhe Chen, and Jin Zhao. Fedac: A adaptive clustered federated learning framework for heterogeneous data. *arXiv preprint arXiv:2403.16460*, 2024.
- [85] Song Lyu, Zheng Lin, Guanqiao Qu, Xianhao Chen, Xiaoxia Huang, and Pan Li. Optimal resource allocation for u-shaped parallel split learning. In *Proc. Globecom Wkshps*, pages 197–202, 2023.
- [86] Zheng Lin, Zhe Chen, Zihan Fang, Xianhao Chen, Xiong Wang, and Yue Gao. Fedsn: A general federated learning framework over leo satellite networks. *arXiv preprint arXiv:2311.01483*, 2023.